



A finite element study of microstructure-sensitive plasticity and crack nucleation in fretting

Title	A finite element study of microstructure-sensitive plasticity and crack nucleation in fretting
Author(s)	McCarthy, Oliver J.;McGarry, J. P.;Leen, Sean B.
Publication Date	2011
Publisher	Elsevier ScienceDirect
Repository DOI	http://dx.doi.org/10.1016/j.commatsci.2011.03.026

A FINITE ELEMENT STUDY OF MICROSTRUCTURE-SENSITIVE PLASTICITY AND CRACK NUCLEATION IN FRETTING

O. J. McCarthy, J. P. McGarry, S. B. Leen
Mechanical and Biomedical Engineering,
NUI Galway, Ireland

Abstract: This paper is concerned with finite element modelling of microstructure-sensitive plasticity and crack initiation in fretting. The approach adopted is based on an existing method for microstructure-sensitive (uniaxial) fatigue life prediction, which proposes the use of a unit cell crystal plasticity model to identify the critical value of accumulated plastic slip associated with crack initiation. This approach is successfully implemented here, using a FCC unit cell crystal plasticity model, to predict the plain low-cycle fatigue behaviour of a stainless steel. A crystal plasticity frictional contact model for stainless steel is developed for microstructure-sensitive fretting analyses. A methodology for microstructure-sensitive fretting crack initiation is presented, based on identification of the number of cycles in the fretting contact at which the identified critical value of accumulated plastic slip is achieved. Significant polycrystal plasticity effects in fretting are predicted, leading to significant effects on contact pressure, fatigue indicator parameters and microstructural accumulated slip. The crystal plasticity fretting predictions are compared with J_2 continuum plasticity predictions. It is argued that the microstructural accumulated plastic slip parameter has the potential to unify the prediction of wear and fatigue crack initiation, leading in some cases, e.g. gross slip, to wear, via a non-localised distribution of critical crystallographic slip, and in other cases, e.g. partial slip, to fatigue crack initiation, via a highly-localised distribution of critical crystallographic slip with preferred orientation (cracking locations and directions).

1 Introduction

Fretting is a phenomenon that occurs when two materials come into contact under a normal load and experience a small relative displacement, typically in a range of 5 to 100 μm , due to vibrations or some other force. It can occur in a wide range of engineering applications such as biomedical, aerospace and oil. Examples include turbine root connections, spline couplings [1] and osteosynthesis plates and screws [2]. Fretting fatigue is dependent on a number of different parameters such as normal load, slip amplitude, surface roughness and surface geometry [3]. The complex nature of this phenomenon makes component life difficult to predict. Three different sliding regimes relevant to fretting are gross slip, partial slip and mixed slip, dependant on slip amplitude for a fixed normal load and coefficient of friction (COF). The main differences between the three regimes can be described in terms of the resulting fatigue and wear. Gross slip generally leads to a high volume of wear, via distributed micro-cracking of asperities for example, and a long fatigue life, while partial slip has a low material wear volume and a short fatigue life due to crack nucleation, commonly in the slip region or at the stick-slip interface [4], and crack propagation. The mixed slip regime combines both slip conditions and generally evolves from gross slip to partial slip. Vingsbo and Soderberg describe the relationship between the three slip regimes, slip amplitude and fatigue life using a "fretting map" [5]. This "fretting map" represents the inter-dependence of fatigue life and wear rate for a given slip regime. Madge *et. al.* [4] were the first to successfully predict the effect of slip on fatigue life, by modelling the effects of material removal on fatigue damage accumulation. The effect of wear on life prediction is less significant in the partial slip regime than in the gross slip regime. In the work of Madge *et al.* [4], the emphasis was on so-called total life, N_f , i.e. not specifically distinguishing between crack initiation life, N_i , and propagation life, N_p , with $N_f = N_i + N_p$. In a separate paper, Madge *et al.* [6] made an attempt to back-calculate modified fatigue (Smith-Watson-Topper) strain-life constants corresponding to 10 μm crack nucleation, using a short crack growth methodology and Paris growth for longer cracks, based on strain-life data corresponding to long cracks, e.g. 1 mm, in an effort to derive fatigue constants which were more consistent in terms of length scales with typical integration point depths in a fretting wear-fatigue predictive model.

1 Ding *et. al.* [7] present significant additional progress by experimentally identifying the
2 numbers of cycles to crack initiation, N_i , to within about 100,000 cycles, in a fretting wear test
3 configuration (i.e. without substrate fatigue load) and successfully predicting crack initiation, to
4 within the same number of cycles, and crack location(s) via a finite element (FE) model that
5 incorporated material removal with a critical plane Smith Watson Topper (SWT) approach as a
6 fatigue indication parameter (FIP) and Miner's rule for damage accumulation. It was argued that the
7 absence of the substrate fatigue load permits more ready identification of crack initiation and fretting
8 wear interaction. However, in the work of Ding *et al* [7], it was necessary to assume that continuum
9 isotropic J_2 plasticity could be employed even for dimensions comparable to grain sizes and,
10 furthermore, it was necessary to assume the same 'back-calculated' 10 μm fatigue constants as
11 employed by Madge *et al.* [6]. Previous work has shown that fretting crack nucleation in partial slip is
12 inherently localised, due to highly localised plasticity and damage, both with respect to depth into the
13 substrate and extent across the surface, so that the applicability of isotropic J_2 plasticity is
14 questionable. For example, typical identified nucleated crack lengths in fretting tests on Ti-6Al-4V
15 [1], specifically designed to capture crack nucleation, were of the same order as the grain size (20 to
16 50 μm). Therefore the use of crystal plasticity (CP) within a fretting FE model is a next logical step
17 for modelling of crack initiation in fretting.
18

19 CP theory [8] models the deformation of individual metallic grains and in particular includes
20 the effects of crystallographic orientation and crystal slip systems. Commonly, rate-dependant single
21 crystal theory is utilized, for example, in the work of McHugh and Connolly [9], McGarry [10] and
22 Huang [11]. Harewood and McHugh [12] used a CP microstructural model to study the failure of a
23 stent under tension and bending. McDowell and Dunne [13] have recently presented a review paper
24 on the topic of microstructure-sensitive fatigue modelling which deals with the crack nucleation and
25 growth at a size scale equal to that of metallic grains.
26

27 Previous work on the application of polycrystal plasticity to modelling of fretting fatigue, i.e.
28 a fatigue specimen with a substrate fatigue load and tangentially-loaded fretting pads, has been
29 presented by Goh, McDowell and co-workers, [13-15] in a series of papers on fretting fatigue of Ti-
30 6Al-4V. Goh *et al* [14] employed a constitutive CP model similar to that employed here, but with
31 inclusion of a back stress term of the Frederick-Armstrong type. The importance of CP in fretting was
32 highlighted, in terms of the significant differences in critical-plane FIPs, e.g. SWT, Fatemi-Socie,
33 between CP and J_2 plasticity, when these FIPs are based on plastic strains as opposed to total strains.
34 It was also pointed out that the use of CP facilitated the prediction of mixed stick-slip zones, due to
35 variations of yielding associated with crystallographic orientation of surface grains and the
36 development of a natural surface roughness from an initially smooth surface without the need to
37 employ an ad hoc asperity distribution and size. The degree of plasticity was predicted to be relatively
38 insensitive to fretting pad pressure, which was argued to be consistent with experiments indicating
39 fatigue life insensitivity to pad pressure. Furthermore, the CP predictions were shown to give
40 significantly better qualitative correlation with experiments in terms of cracking locations, angles etc
41 than J_2 plasticity. Later work by the same group [15], focussed on normal loads greater than or equal
42 to the yield load, emphasised the significantly larger degree of plastic deformation predicted by
43 viscoplastic CP analyses of fretting of Ti-6Al-4V (than J_2) and proposed an important role of plastic
44 ratchetting strain in fretting. More recent work again [16] on microstructure effects in fretting via CP
45 modelling of Ti-6Al-4V concluded that average grain size and crystallographic orientation have more
46 influence on fretting fatigue behaviour, as characterised via the Fatemi-Socie FIP, than grain size
47 distribution, while Zhang *et al.* [17] introduced a ratchetting strain based, critical-plane FIP to
48 quantify the relative dependence of fretting-induced plasticity (without actually predicting numbers of
49 cycles to initiation) on fretting loading parameters, under tangential load control, i.e. only partial slip.
50

51 One of the challenges associated with fretting fatigue is the prediction of crack initiation. An
52 approach devised by Manonukul and Dunne [18] allowed prediction of the LCF and HCF material
53 response for a nickel base alloy C263. A critical accumulated plastic slip parameter predicted when
54 crack initiation occurred in a crystal plasticity aggregate. The key significance of this approach is the
55 potential to predict the effects of microstructural features, such as inhomogeneities and material
56 defects, on fatigue crack initiation.
57
58
59
60
61
62
63
64
65

This paper is concerned with the development of a computational method for prediction of microstructure-sensitive crack nucleation in fretting. The approach is demonstrated for plain (low-cycle) fatigue and fretting of 316L stainless steel. 316L SS is a widely-used material for medical implants, e.g. prosthetic hip stems, and the phenomenon of fretting is observed clinically in biomedical implants, e.g. osteosynthesis plates and screws [2]. A better understanding of fretting crack initiation at a microstructural level will lead to better design of implants. The microstructure sensitive approach is based on a CP unit cell model and CP frictional contact model. The CP fretting predictions are compared with J_2 plasticity in terms of predicted evolution and distributions of surface and sub-surface variables, including contact pressure, surface shear, relative slip and FIP (critical-plane SWT), across a range of key fretting variables, such as normal load (contact size) and applied tangential displacement. The comparative performance of the CP-based microstructure sensitive methodology is compared with the more widely used J_2 -based methods (in this case, critical-plane SWT method) with respect to crack nucleation prediction.

2 Methodology

2.1 Crystal plasticity theory

The crystal plasticity theory [8] used in this paper is a physically based, rate dependant crystallographic theory that models the deformation of a metallic crystal lattice. The total deformation in a crystal lattice can be described by the deformation gradient \mathbf{F} . The following equation describes (using standard tensor notation throughout) the decomposition of the deformation gradient \mathbf{F} into its elastic \mathbf{F}^e and plastic \mathbf{F}^p parts

$$\mathbf{F} = \mathbf{F}^e \cdot \mathbf{F}^p \quad (1)$$

where \mathbf{F}^e typically represents the rigid body rotation and elastic deformation of the crystal lattice and \mathbf{F}^p represents the plastic shear flow through the material. However both the elastic and plastic deformation gradients may contain stretch and rigid body rotation. The velocity gradient \mathbf{L} is defined through the following where the dot represents a time derivative.

$$\mathbf{L} = \dot{\mathbf{F}} \cdot \mathbf{F}^{-1} \quad (2)$$

$$= (\dot{\mathbf{F}}^e \cdot \mathbf{F}^p + \mathbf{F}^e \cdot \dot{\mathbf{F}}^p) \mathbf{F}^{-1} \quad (3)$$

$$= \dot{\mathbf{F}}^e \cdot \mathbf{F}^p \cdot (\mathbf{F}^p)^{-1} \cdot (\mathbf{F}^e)^{-1} + \mathbf{F}^e \cdot \dot{\mathbf{F}}^p \cdot (\mathbf{F}^p)^{-1} \cdot (\mathbf{F}^e)^{-1} \quad (4)$$

$$= \mathbf{L}^e + \mathbf{L}^p \quad (5)$$

The elastic and plastic velocity gradient, \mathbf{L}^e and \mathbf{L}^p are defined as follows:

$$\mathbf{L}^e = \dot{\mathbf{F}}^e \cdot (\mathbf{F}^e)^{-1} \quad (6)$$

$$\mathbf{L}^p = \mathbf{F}^e \cdot \dot{\mathbf{F}}^p \cdot (\mathbf{F}^p)^{-1} \cdot (\mathbf{F}^e)^{-1} \quad (7)$$

The velocity gradient \mathbf{L} can be decomposed into the deformation rate, \mathbf{D} , and the spin tensor, \mathbf{W} ,

$$\mathbf{L} = \mathbf{D} + \mathbf{W} \quad (8)$$

where

$$\mathbf{D} = \frac{1}{2}(\mathbf{L} + \mathbf{L}^T) \quad (9)$$

$$\mathbf{W} = \frac{1}{2}(\mathbf{L} - \mathbf{L}^T) \quad (10)$$

$$\mathbf{D} = \mathbf{D}^e + \mathbf{D}^p \quad (11)$$

$$\mathbf{W} = \mathbf{W}^e + \mathbf{W}^p \quad (12)$$

Plastic slip is assumed to obey Schmidt's law [8], where the rate of plastic shear strain, $\dot{\gamma}^\alpha$, for a particular slip system, α , is assumed to depend on the resolved shear stress, τ^α , through the following power law:

$$\dot{\gamma}^\alpha = \dot{a} \operatorname{sgn}(\tau^\alpha) \left\{ \left| \frac{\tau^\alpha}{g^\alpha} \right| \right\}^n \quad (13)$$

where \dot{a} and n are the reference strain rate and rate sensitivity exponent, respectively. Material strain hardening is specified by the slip system strain hardness, g^α , which is defined by the integral of the following equation:

$$\dot{g}^\alpha = \sum_{\beta} h_{\alpha\beta} \dot{\gamma}^\beta \quad (14)$$

where $h_{\alpha\beta}$ are the strain hardness moduli and $h_{\alpha\alpha}$ and $h_{\alpha\beta}$ are the self and latent hardening moduli, respectively. In this work Taylor isotropic hardening is assumed and self and latent hardening moduli are considered equal. $g(\gamma_\alpha)$ is the slip system strain hardness defined by the following hardness function [19]:

$$g(\gamma_\alpha) = g_0 + (g_\infty - g_0) \tanh \left| \frac{h_0 \gamma_\alpha}{g_\infty - g_0} \right| \quad (15)$$

where h_0 is the initial hardening modulus, g_∞ is the saturation stress and g_0 is the critical resolved shear stress. The hardening moduli can be found through differentiation of the above equation, as follows:

$$h_{\alpha\alpha} = h_{\alpha\beta} = h(\gamma) = h_0 \operatorname{sech}^2 \left| \frac{h_0 \gamma_\alpha}{g_\infty - g_0} \right| \quad (16)$$

The accumulated slip, γ_α is defined as follows:

$$\gamma_\alpha = \sum_{\alpha} \int_0^t |\dot{\gamma}^\alpha| dt \quad (17)$$

This theory is implemented here in Abaqus 6.9 via a user defined material, (UMAT) user subroutine following the approach of [11].

2.2 CP model calibration

316L stainless steel has a face centred cubic, (FCC), crystalline structure which consists of 12 slip systems. The geometry within the crystal lattice is described in terms of 4 slip planes each with 3 slip directions described by the Miller indices, $\langle 111 \rangle \{110\}$. In this work isotropic elasticity is assumed within the CP user subroutine, with a Young's modulus of 209 GPa and Poisson's ratio, ν , of 0.28. The unit cell model shown in Figure 1 represents the metallic crystal grains at a microstructural level. A grain size of $d = 104 \mu\text{m}$, based on the 316L stainless steel of [20] is modelled using an assumed regular hexagonal grain morphology, following the work of Savage et al. [21]. This permits inclusion of triple points, at grain boundary intersections, which is an important feature in microstructure modelling and CP deformation. Random crystallographic orientations, which are kept consistent throughout the calibration process, are assigned to individual grains.

The unit cell approach represents a repeating unit of a microstructure in a uniaxial fatigue specimen. The unit cell model consists of 42 uniform whole hexagonal grains and 22 other partial grains making up the grain boundaries. Four-noded, plane strain elements are used throughout this work. Symmetry boundary conditions are employed on the left and bottom edges of the unit cell and the right and top edges are constrained to remain straight.

An important issue in CP modelling is the identification of constitutive parameters. In this paper, the CP parameters are identified using the macroscopic cyclic stress-strain curve (CSSC) of 316L, as represented by a non-linear kinematic hardening material J_2 model, using the material data shown in Table 1, from [22]. The initial hardening modulus, h_0 , saturation stress, g_∞ , and critical resolved shear stress, g_0 , were identified using an iterative approach with respect to correlation of the unit cell model cyclic response to the macroscopic cyclic response, across a range of applied strain-ranges. Figure 2 shows the predicted stabilised hysteresis loops for the CP unit cell model for a range of different strain ranges. Figure 3 shows a comparison of the CP stabilised CSSC, using the identified CP constitutive constants, as given in Table 2, with the macroscopic (aggregate) CSSC for 316L; although there is not exact correlation, the fit is considered sufficiently accurate. \dot{a} and n were set to $0.001s^{-1}$ and 20, respectively, for this identification process and for subsequent use in this paper. This also provided a reasonable convergence time for the analysis. Stabilisation (to within 2%) of the CP cyclic stress-strain loops occur within less than 20 cycles.

2.3 Microstructural sensitive crack initiation parameter

Manonukul and Dunne [18] proposed a new microstructural parameter, accumulated plastic slip, p , as the key parameter controlling crack initiation for low and high cycle fatigue. p is defined in terms of an effective plastic slip rate as follows:

$$\dot{p} = \left(\frac{2}{3} \mathbf{L}^p : \mathbf{L}^p\right)^{\frac{1}{2}} \quad ; \quad p = \int_0^t \dot{p} dt \quad (18)$$

where the plastic velocity gradient \mathbf{L}^p is defined by:

$$\mathbf{L}^p = \sum_{\alpha=1}^n \dot{\gamma} \mathbf{s}^\alpha \mathbf{n}^{\alpha T} \quad (19)$$

with \mathbf{s}^α and \mathbf{n}^α as the slip direction and normal vectors, respectively, for a given slip system, α , with n slip systems. \dot{p} and p are coupled in the CP user subroutine. The criterion for crack initiation presented in [18] is $p = p_{crit}$. As pointed out in [18], with calculation of the maximum accumulated slip, together with knowledge of the experimentally determined number of cycles to failure, N_f , for a particular test with known loading conditions, it is possible to determine p_{crit} . Figure 4 shows the predicted distribution of p for an applied strain range of 2%, illustrating the localised nature of the distribution. Due to the quick stabilisation of the stress-strain response [18] it is possible to determine a stabilised maximum accumulated plastic slip per cycle, p_{cyc} . The crack initiation criterion is then written as [18]:

$$p_{crit} = N_i p_{cyc} \quad (20)$$

The critical accumulated slip, p_{crit} , was argued to be a fundamental quantity and was shown in [18] to be able to predict the occurrence of crack initiation over a range of temperature and for both low cycle fatigue (LCF) and high cycle fatigue (HCF) for C263, a FCC nickel alloy. In general, it is not easy to determine N_i , but it is relatively easy to determine N_f . Hence, if $N_i \approx N_f$, as was argued for the C263 material in [18], p_{crit} can be determined from N_f . In the present paper, it is argued that for LCF, it can be assumed that $N_i \approx N_f$, i.e. N_p is small relative to N_i so that p_{crit} can be determined from N_f for a LCF test. In the present paper for the 316 L stainless steel material considered here, the measured experimental LCF response of the material is encapsulated by the Coffin-Manson relationship between predicted number of cycles, N_f , and plastic strain range, $\Delta\varepsilon_p$, as follows:

$$N_f = \left(\frac{\Delta \varepsilon_p}{\varepsilon_{f'}} \right)^{\frac{1}{c}} \quad (21)$$

where $\varepsilon'_{f'}$ and c are material constants given in Table 3. The p_{crit} value, describing microstructural crack initiation for 316 L stainless steel here, is then identified using the N_f value corresponding to one particular value of plastic strain range, $\Delta \varepsilon_p$. The p_{crit} value thus identified is 58.8. This identified p_{crit} value is then validated by using it, (along with Equation 20), and the results of the unit cell model for a range of applied strain ranges, to predict the LCF response across the range of applied strain ranges. Figure 5 shows a comparison between the resulting CP unit cell LCF predictions and the Coffin-Manson relationship for stainless steel (using the constants of Table 3). It is clear that the identified p_{crit} value gives good correlation with the measured Coffin-Manson relationship. This identified value of p_{crit} is subsequently applied (below) to the prediction of fretting crack nucleation for 316L SS, for a cylinder-on-flat fretting wear configuration in the following sections.

2.4 Total life prediction

As mentioned in the Introduction, previous work on prediction of fretting crack initiation has focussed on the use of a class of parameters now referred to as fatigue indication parameters, examples of which are SWT, Fatemi-Socie (FS), Dang Van and Walker. Within a fretting context, these parameters are commonly evaluated on the basis of a critical-plane approach, as described below, to deal with the multiaxial stresses and strains in fretting. These methods are considered to be total life methods, since they are generally predicated on predicting a number of cycles (or reversals) to a 1 mm surface crack, e.g. see Socie [23]. The choice of which FIP to use, according to Socie, should be based on consideration of material (fatigue) cracking behaviour, viz. Mode I (tensile) cracking or Mode II (shear) cracking. For Mode I failures, Socie recommends the SWT parameter and for Mode II failures the FS parameter. As pointed out by Socie [23], in relation to materials such as 304 stainless steel (assuming 316L can be similarly classed), which mode pertains depends on stress state and cyclic strain amplitude. Socie points out that Mode I failures occur for all strain amplitudes in tensile loading and for low strain amplitudes in shear loading. On the assumption that fretting contact regions for 316L stainless steel experience a combination of tensile and low strain shear cyclic loading, it is assumed here that the SWT parameter can be used to provide estimates of total life, N_f , defined here in the context of FIP constants corresponding to a 1 mm surface crack. The SWT parameter and life prediction equation can be expressed as follows:

$$SWT = \sigma_{\max} \frac{\Delta \varepsilon}{2} = \frac{(\sigma_{f'})^2}{E} (2N_f)^{2b} + \sigma_{f'} \varepsilon_{f'} (2N_f)^{b+c} \quad (22)$$

where $\sigma_{f'}$ is the fatigue strength coefficient, $\varepsilon_{f'}$ is the fatigue ductility coefficient, b is the fatigue strength exponent, c is the fatigue ductility exponent and E is Young's modulus. The values of these constants for 316L, tabulated in Table 3, are obtained from Lemaitre and Chaboche [22]. The SWT approach spans across both LCF and HCF, including mean stress effects and also additional strain hardening associated with out-of-plane loading, as displayed by materials such as stainless steel [22]. A critical-plane approach is adopted for evaluation of the SWT parameter acknowledging the fact that cracks can initiate and grow on planes at any angle to the loading axis. SWT predicts the 'damage' per cycle on any given plane orientation for a given loading cycle. The parameter combines the peak normal stress, σ_{\max} , within one cycle and the strain range, $\Delta \varepsilon$, which is defined as the difference between the maximum and minimum strain within a cycle. The critical-plane approach involves maximisation of the SWT parameter with respect to potential cracking plane, using 5° intervals over a range of 180° . A more detailed description of the methodology implemented here can be found in Sum et al. [24]. The SWT critical plane approach has produced realistic predicted results compared to experimental results for plain and fretting fatigue of a high strength CrMoV aeroengine steel [24, 25] and for fretting fatigue of Ti6Al4V [4,6]. In this paper, it is argued that, for crack initiation prediction, it is necessary to use a microstructural parameter, such as the p_{crit} parameter described above. Hence,

1 the primary purpose of the FIP is to provide total life estimates in fretting, against which to compare
2 predicted initiation lives, the use of alternative FIPs would be expected to give broadly similar results
3 and trends.

4 2.5 Cylinder-on-flat fretting model

5 Figure 6 shows a schematic of the crossed cylinder-on-flat fretting rig modelled in the present study,
6 which is the University of Nottingham fretting test rig described in more detail in previous work, e.g.
7 [3]. The cylindrical specimen is pressed against the flat specimen under a dead weight and oscillated
8 tangentially under displacement (stroke) control. This differs from fretting fatigue tests which have a
9 (cyclic) fatigue load applied to the fretted substrate. It is argued here that the substrate fatigue load is
10 an additional and unnecessary complication in terms of identification and decoupling of crack
11 nucleation from crack propagation, so that a fretting wear configuration is more fundamentally suited
12 to identification of fretting crack initiation/nucleation. This arrangement has been successfully used
13 by McColl et al. [3] to experimentally characterise the fretting wear behaviour of a high strength,
14 CrMoV aeroengine steel and thence to validate a novel wear simulation technique under different
15 normal loads and stroke combinations. It has also been used, more recently, by Ding et al. [7], to
16 characterise the fretting wear and crack initiation behaviour of Ti6Al4V, e.g. see Figure 7, across
17 different fretting slip regimes, and as mentioned in the Introduction, to validate J_2 -based, SWT
18 predictions of crack initiation, including the effects of wear simulation, i.e. material removal.

19 In this paper, following the approach of previous studies, e.g. [3], this experimental
20 arrangement is modelled using a 2D plane strain, cylinder-on-flat frictional contact model, as shown
21 in Figure 8, consisting of a 6 mm radius (R) 316L pad on a 5×10 mm 316L substrate. The bottom
22 surface of the substrate is constrained in the X and Y directions. Linear constraint equations are
23 specified between a single node on the top surface of the pad and the other top surface nodes, to
24 constrain the top surface to have uniform displacements in the vertical and horizontal directions. The
25 normal load P is applied in a first step and held constant thereafter, to simulate the experimental
26 application of the dead-weight load; subsequently, a cyclic tangential displacement δ_{app} is applied to
27 the pad top surface. The frictional contact modelling approach employed follows that presented in
28 previous work, e.g. [7]. In the unlubricated fretting of metallic surfaces, such as steel or titanium, the
29 COF commonly starts off low, at about 0.3 and increases with number of fretting cycles to a stable
30 value between 0.7 to 1.0 or higher, depending on many factors including normal load, stroke, material
31 compositions etc. Consequently, in the present study, a representative COF value (μ) of 0.8 is
32 adopted. The Lagrange multiplier frictional contact algorithm is employed with Abaqus to enforce an
33 exact sticking constraint between the two surfaces when the shear stress (τ) is less than the critical
34 shear stress, i.e. $\tau < \mu p$, where p is the local (nodal) contact pressure.

35 Two different material modelling approaches are adopted here in the fretting model as
36 follows:

- 37 (i) a J_2 NLKH material model (referred to hereafter as the ‘ J_2 fretting model’) throughout all of
38 the substrate, using the material properties defined in Table 1.
- 39 (ii) a hybrid material model (referred to hereafter as the ‘CP fretting model’), consisting of a CP
40 material model in the contact region (see Figure 8b), using the material properties defined in
41 Table 2, and J_2 NLKH material model outside of this region, using the properties of Table 1.

42 The CP fretting model is designed on the basis of square grains in place of hexagonal grains, for better
43 control of the mesh design in critical contact region. Comparison between both square and hexagonal
44 grains was made using the unit cell approach. The unit cell consisting of square grains was generated
45 in a similar fashion to the hexagonal grains. Grain area, number of elements per grain, orientation and
46 position were kept consistent between the two analysis as well as all boundary conditions and
47 constraints. The position of the square grains allowed the modelling of triple points as seen between
48 the hexagonal grains; this is characteristic of real microstructures. Figure 9 shows a comparison of the
49 predicted accumulated plastic slip (p) distributions for the two different grain geometries at an applied
50 (cyclic) strain range of 2%. The contour plots show almost identical locations of localised plastic slip
51 and maximum values of p . Furthermore, the predicted hysteresis loops from the square grain and
52 hexagonal grain microstructure unit cell models were identical across the range of strain ranges.

In any methodology involving FE modelling, the design of mesh is important. In the analyses of the steep stress gradients associated with fretting problems, the mesh design is critical to accuracy and reliability of predictions. In the model of Figure 8, a dense mesh is used in the contact regions for optimum accuracy where significant stress gradients are anticipated, leading to plasticity under tangential loading, while a coarser mesh is used away from the contact regions to optimise with respect to computational overhead; this is particularly onerous in the case of the CP fretting analyses. A mesh refinement study has been conducted to establish the optimum degree of mesh refinement in the contact regions with respect to plasticity prediction. This study was based on the use of the J_2 fretting model and total life prediction using the critical plane *SWT* approach, across a range of applied tangential displacements, for successively increasing mesh refinement in the contact regions. An initial coarse mesh of 13 μm square elements was used followed by further refinement, using 8.67 μm , 6.5 μm and 3.25 μm square elements. Figure 10 shows (i) the decreasing total life with increasing applied displacement and (ii) the decreasing total life with increasing mesh refinement. Based on these results, a 6.5 μm square element size is employed here as a good compromise between accuracy and computational expense. The same mesh design is used for both the J_2 fretting model and the CP fretting model. The crystal plasticity region of the CP fretting model contains a 7×33 mesh of square grains (i.e. 231 grains in total), each of side length 104 μm . Each grain thus contains 256 square elements. Random orientations assigned to each grain were kept constant throughout the subsequent CP fretting analyses. The vertical dimension of the surface grain is 50% of the horizontal dimension.

As mentioned above, normal load is a key variable in fretting and has been shown in previous work to be particularly important in plasticity analyses of fretting, e.g. [26]. The normal load to cause yielding on cylinder on flat contact is given by the following equation [27]:

$$P_y = \frac{\pi R}{E^*} (p_o)_Y^2 \quad (23)$$

where

$$(p_o)_Y = 1.8k \quad (24)$$

where R is the radius of the pad, E^* is the composite modulus and k is the yield stress of the material.

3 Fretting model results

Two of the key (running condition) loading variables controlling fretting wear and fatigue are normal load and applied stroke (tangential displacement). Two normal loads are considered in the fretting analyses presented here, an ‘elastic’ case with $P = 0.5P_y$ and a ‘plastic’ case with $P = 2P_y$. For each of these, a range of applied displacements are investigated, between 0.5 μm and 2 μm , typically spanning from partial slip to gross slip, for both fretting models. The objective is to present a comparative assessment of plasticity predictions from both material models, with particular emphasis on the implications for prediction of crack nucleation and initiation. Previous work has highlighted the importance of contact pressure evolution on wear [3] and fatigue damage [4] accumulation in fretting. Shear stress plays a key role in fatigue crack initiation and in fretting, this means contact shear stresses. Relative slip (with shear and contact pressure) in contact is a distinguishing variable for fretting surface damage, which undoubtedly leads to premature crack initiation relative to plain fatigue situations. Therefore, the effects of material modeling on the predicted distributions, trends and values of these variables are central to the development of novel methods for prediction of crack initiation and wear in fretting.

Figure 11 and Figure 12 show the predicted evolutions of contact pressure within the first twelve tangential loading cycles for both fretting models and across a range of applied displacements. The $N = 0$ curve corresponds to normal loading only before any tangential displacements occur. Table 4 and 5 summarise the predicted slip regimes and evolution of contact widths. A number of observations can be made from these results as follows:

1. For the J_2 model, the initial $N = 0$ distributions for $0.5P_y$ (Figs. 11a, 11c, 11e) correspond identically to the Hertzian distributions. Even for $0.5P_y$, it is clear that the NLKH material model predicts a significant effect of tangential friction-induced plasticity on the contact pressure distribution and contact width, resulting in as much as a 25% drop in peak pressure

and as much as 25% increase in contact width, for gross slip cases. Comparative analyses for $\mu = 0$ and 0.3 confirmed that the plasticity is tangentially induced by frictional effects (results not shown here). Under partial slip, e.g. $\delta_{\text{app}} = 0.5 \mu\text{m}$, negligible plasticity effects are predicted for the $0.5P_y$ normal load.

2. For the J_2 model, with $2P_y$, (Figs 12a, 12c, 12e), the predicted effect of plasticity on contact pressure and contact width increases with increasing stroke, with up to 40% increase in contact width and up to 25% drop in peak pressure. In this case, the initial ($N = 0$) ‘plastic’ distribution of pressure is clearly non-Hertzian.
3. The predicted effect of frictionally-induced plasticity is more complex and more significant for the CP fretting model. First of all, even for the ‘elastic’ case of $0.5P_y$, the $N = 0$ distribution is non-Hertzian (Figs. 11b, 11d, 11f) and, although the predicted initial contact widths are the same as the J_2 and Hertzian models, the predicted peak pressures are up to 10% lower. Note that in this case, the contact width is only about one grain wide (viz. about $100 \mu\text{m}$). For the $2P_y$ case, the initial ($N = 0$) contact pressure distribution (Figs 12b, 12d, 12f) is now significantly different to both the Hertzian and the corresponding J_2 model. Also, the contact widths are now no longer precisely symmetric due to material inhomogeneity. The key differences are (i) the significantly more non-smooth (inhomogeneous) distribution, (ii) the significantly larger ($\sim 27\%$) contact width, and (iii) the significantly lower ($\sim 15\%$) peak pressure. The occurrence of (i) is attributed to the development of a natural surface roughness (see also [14]) in the material, due to differential yielding across the different grains in the contact width. In this case, the contact width is about two grains wide.
4. The CP-predicted contact widths, under frictionally-induced plasticity, increase significantly by up to 94% (i.e. almost doubling in width), with significantly larger predicted increases for the $0.5P_y$, normal load.
5. Furthermore, the predicted CP pressure distributions show (i) significant redistributions of pressure so that the peak pressures reduce significantly by up to 60%, while new material comes into contact, with associated increased pressure in these new contact regions, and (ii) development of a more inhomogeneous distribution (i.e. more noisy) with increasing plasticity (fretting cycles).

Figure 13 and Figure 14 show the corresponding evolutions of contact shear distributions. The $N = 1$ curve corresponds to the first tangential displacement cycle. Some key observations related to these are as follows:

1. The J_2 shear tractions for $0.5P_y$ (Figs 13a, 13c, 13e) show (i) that the predicted contact width increase in general occurs within the first tangential displacement cycle, i.e. $N = 1$, (ii) the characteristic partial slip shear traction distribution for a Hertzian contact for $\delta_{\text{app}} = 0.5 \mu\text{m}$, which is unaffected by plasticity, consistent with the corresponding pressure distribution evolution and (iii) that the effect of plasticity on the gross slip shear traction distributions of the $1 \mu\text{m}$ and $2 \mu\text{m}$ δ_{app} cases follows the corresponding contact pressure trends of Figs. 11c and 11e; it is worth noting that the NLKH J_2 model predicts shear redistribution (including reducing peak shear) even between cycles 6 and 12. Clearly, the shear tractions are predicted to increase with increasing stroke, saturating with respect to slip once the partial to gross slip threshold is exceeded.
2. The J_2 shear tractions for $2P_y$ (Figs 14a, 14c, 14e) clearly show partial slip characteristic distributions for $0.5, 1$ and $2 \mu\text{m}$ δ_{app} values; for the $2 \mu\text{m}$ case, the peak shear traction, corresponding to the stick-slip interface, is predicted to move outwards with increasing cycles, with the final peak occurring at $x \approx \pm a_0$, the initial ($N = 0$) contact edge, whereas for the 0.5 and $1 \mu\text{m}$ cases, the stick-slip interface is unchanged after the first tangential cycle ($N = 1$);
3. For the $0.5 \mu\text{m}$ case, the J_2 predicted peak shear is seen to be higher for the lower normal load ($0.5P_y$); for the $1 \mu\text{m}$ case, this is also true but with a much smaller difference. For the $2 \mu\text{m}$ case, the higher normal load value ($2P_y$) is higher.
4. The CP shear tractions (Figs 13b, 13d, 13f, 14b, 14d, 14f) are, in general quite different to the J_2 distributions. Some of the key differences are as follows: (i) they generally have lower

1 peak values, (ii) the shear is distributed over a larger contact width, consistent with the
2 pressure distributions, (iii) the distributions show significantly more fluctuations with respect
3 to horizontal contact position, with significantly more localised peak values, attributed to
4 inherent microstructural, material inhomogeneity, and (iv) in general, the initial ($N = 1$) high
5 peaks, attributed to the naturally-predicted surface roughness, are re-distributed by localised
6 plastic deformation, leading to final ($N = 12$) broadly-speaking smoother distributions.

7
8 Figure 15 and Figure 16 show the predicted effects of plasticity on the critical-plane SWT
9 distributions along the surface for the J_2 and CP fretting models and Tables 6 and 7 show
10 corresponding key summary data. For both models, plasticity is predicted to have a significant effect
11 on this FIP and hence on predicted N_f . The J_2 model predictions for the $0.5P_y$ (Figs 15a, 15c, 15e)
12 case show that the final ($N = 12$) maximum SWT increases with δ_{app} and saturates at a maximum
13 value at $\delta_{app} = 1 \mu\text{m}$, so that the predicted N_f levels off at that displacement also; for the $2P_y$ (J_2
14 model) case (Figs 16a, 16c, 16e) the SWT values are lower than for $0.5P_y$ for $\delta_{app} \leq 1 \mu\text{m}$, but become
15 greater for higher δ_{app} values and the predicted N_f does not level off, but continues to decrease, due to
16 the non-occurrence of gross slip for $\delta_{app} \leq 2 \mu\text{m}$. Hence, the J_2 model predicts significantly lower N_f
17 for $2P_y$ for $\delta_{app} \geq 1.5 \mu\text{m}$. In general, the J_2 model predicts the peak FIP values at or very close to the
18 contact edge, for both partial and gross slip cases.

19
20 It is also of interest to use the CP model to predict N_f using the critical-plane SWT (FIP)
21 approach (Figs 15b, 15d, 15f, 16b, 16d, 16f). The CP model predicts very similar SWT N_f values to
22 the J_2 model but the peak SWT (failure) location is in general different and is away from the contact
23 edge in some cases, e.g. for $\delta_{app} = 0.5, 1$ and $2 \mu\text{m}$ for $0.5P_y$, and at the contact edge, e.g. $\delta_{app} = 1.5$
24 μm for $2P_y$.

25
26 Figures 17 (a) and (b) show the predicted variation of N_f with δ_{app} for $0.5P_y$ and $2P_y$. Both
27 models show broadly similar trends, with the CP model showing some scatter relative to the J_2 model,
28 as expected, given the specified random crystallographic orientations of the grains and hence yield
29 strengths. For Figure 16 the CP model shows some dramatically higher initial ($N = 1$) SWT values
30 which are re-distributed with plastic deformation. These are attributed to the development of a natural
31 surface roughness, alluded to earlier, and associated significant local peaks in pressures and shears
32 and associated substrate stress components.

33
34 Figure 18 shows the CP predicted surface distributions of p_{cyc} . These distributions are, in
35 general, broadly similar to the FIP distributions with localised peak values generally occurring away
36 from the central contact region. However, unlike the FIP distributions, the peak values for $0.5P_y$
37 always occur well away from the contact edge, under the contact, while the peak values for $2P_y$ are
38 closer to the contact edge, except for low δ_{app} . Significant changes (reductions) in p_{cyc} are predicted
39 between the 6th and 12th cycles. p_{cyc} is predicted to saturate also for gross slip cases but still has a
40 random (inhomogeneous) nature, leading to different values even for nominally saturated (gross slip)
41 conditions. p_{cyc} is predicted to be higher for the lower normal load when $\delta_{app} \leq 1.25 \mu\text{m}$ (see Tables 8
42 and 9).

43
44 Figure 19 shows the predicted contour plots of p after 12 tangential cycles for $0.5P_y$ and $2P_y$
45 and different δ_{app} values. It can be deduced from Figure 19 (and Figure 18) that two types of
46 distributions of the crack initiation parameter, p , can be identified. The first (Type 1), as displayed by
47 $\delta_{app} = 0.5 \mu\text{m}$ and $1 \mu\text{m}$ for $2P_y$ (Figs 19b, 19d), is characterised by localised contours of p (and p_{cyc}),
48 aligned with preferred directions, making acute angles of $\approx 48^\circ - 53^\circ$, consistent with typical fretting
49 crack directions (e.g. see Figure 7; experimental data shows cracks to occur at similar angles between
50 40° to 60° [14]) and of length about one or two grains, again consistent with observed short cracks in
51 fretting. The second type (Type 2) of distribution of crack initiation parameter, p (and p_{cyc}), is
52 significantly more uniform over a region resembling a typical wear scar shape, either (i) over a small
53 region of about one grain length by one quarter of a grain length, e.g. $\delta_{app} = 0.5 \mu\text{m}$, 1 and $2 \mu\text{m}$ for
54 $0.5P_y$ (Figs 19a, 19c, 19e), or (ii) over a much larger region of two or three grain lengths by about one
55 grain depth, e.g. $\delta_{app} = 2 \mu\text{m}$ for $2P_y$ (Fig 19f). It is argued here that these two types of distribution
56 demonstrate that the microstructural crack initiation parameter, p_{crit} , has the ability to permit
57 differentiation between (i) localised crack nucleation leading ultimately to fatigue cracking (Type 1)
58
59
60
61
62
63
64
65

and (ii) uniform micro-cracking leading to wear (Type 2), which may or may not ultimately lead to fatigue cracking, depending again on substrate or superimposed loading (additional to fretting loads).

Figure 20 shows the p_{crit} predicted life for $0.5P_y$ and $2P_y$ over a range of δ_{app} . Comparison between the two normal loads shows (i) a higher predicted life at small δ_{app} for $2P_y$, (ii) decreasing life with increasing δ_{app} for both loads and (iii) higher predicted life at large δ_{app} for $0.5P_y$. The levelling out of predicted life for $0.5P_y$ at the higher δ_{app} is consistent with the change in slip regime from partial slip to gross sliding which has not occurred for $2P_y$. Figure 21 shows comparisons of the predicted numbers of cycles to crack initiation (based on p_{crit}) and to total life (based on critical-plane SWT with CP fretting model) for both the low and high normal loads, over the range of tangential displacements. Of course, these predicted total lives are only indicative, since they do not include a number of factors as follows:

1. they are based on the assumption of no wear, ignoring the possibility of crack arrest due to (i) wear-induced pressure and stress re-distribution [4] or (ii) wear-induced material removal of the cracked material [6].
2. they do not account for precisely the type of initiation prediction encapsulated by p_{crit} , viz. microstructure sensitive crack nucleation, which is the principal subject of this paper,
3. they do not account for short crack growth effects, e.g. see [6], including, for example, possible crack arrest due to lack of sufficient crack driving force.

It can be seen that the predicted N_i values are less than 8000 for the $0.5P_y$ normal load and are relatively insensitive to applied displacement above the transition to gross slip (levelling off at ~ 5000 after gross slip onset), due to effective levelling-off of p_{cyc} . In contrast, the N_i values for the $2P_y$ load decrease from about 27,000 to about 3500 continuously with increasing displacement, due to increasing p_{cyc} value. A key point to note is that the predicted initiation lives are from 0.4% to 1.4% of the predicted total lives for $0.5P_y$ and from 1% to 11% for $2P_y$ for these fretting analyses. Golden and Calcaterra [28] have reported similar proportions of between 1% to 10% of total life for fretting of Ti6Al4V alloy. The calculated numbers of cycles to initiation in that case were between 5,000 and 50,000, which are also consistent with the fretting initiation lives presented here.

The higher predicted life for larger normal load at low δ_{app} values is at first glance non-intuitive, as one might expect increased load to lead to lower lives. The fact that $2P_y$ gives lower lives at high δ_{app} values here, is related to the fact that for $2P_y$, at these δ_{app} values, gross slip has not been achieved, whereas for $0.5P_y$, the gross slip transition occurs at $\delta_{app} = 1 \mu\text{m}$. Hence, for the lower normal load, the shear traction and hence peak shear stresses and, by extension, SWT and p_{cyc} lives, have saturated for $\delta_{app} \geq 1 \mu\text{m}$, whereas for $2P_y$, the shear traction, peak shear stresses and hence SWT and p_{cyc} values continue to increase up to $\delta_{app} = 2 \mu\text{m}$. Thus the predicted lives for $2P_y$ continue to decrease right up to $\delta_{app} = 2 \mu\text{m}$.

The results of Tables 6 to 9 show that the steady-state ($N = 12$) critical-plane SWT and p_{cyc} predictions at low δ_{app} values, e.g. $\delta_{app} \leq 1 \mu\text{m}$, are lower for $2P_y$. Although the theoretical, elastic solutions for shear stress distributions [27] show that the peak shear stress values (at the stick-slip interface) are almost identical for both normal load cases, the elastic-plastic FE predictions of the present work show lower peak shear stress values for $2P_y$. This is attributed to the greater degree of plasticity in the higher normal load case. The lower values of SWT and p_{cyc} at the higher normal load for low δ_{app} values, is therefore attributed here to the effects of plasticity. It is also worth pointing out that the shear stress gradient is significantly higher for the $2P_y$ load case, due to the fact that the slip zone is significantly smaller for this case. The critical-plane approach adopted here, based on that in [24], by virtue of averaging integration point SWT values in each element (for more details see [24]), permits capturing of gradient effects. In [24], this permitted prediction of a contact size effect in fretting fatigue. The same rationale is adopted for the numerical implementation of the p_{cyc} calculations, so that it can also capture a gradient effect.

In terms of experimental evidence for the predicted effects of normal load on life, Zhou et al [29], for example, have shown, that an increase in contact load, for a fixed small tangential displacement (in the partial slip to stick transition regime), leads to an increase in number of cycles to crack nucleation. This is consistent with the trend shown in Figures 17 and 20 for low δ_{app} values, i.e. higher life for higher normal load. On the other hand, in relation to the effect of normal load at the

higher δ_{app} values, Nakazawa et al [30] have shown, through experimental fretting fatigue testing of 316L stainless steel for a punch on flat fretting bridge geometry, that with higher stress amplitudes (which can be considered as equivalent to higher tangential displacements), higher contact pressure (normal load) gives lower life and with reducing stress amplitude (i.e. decreasing tangential displacement) the lives associated with higher and lower normal loads converge. These results are consistent with the results of Figures 17 and 20, for the high and intermediate δ_{app} values, i.e. at high δ_{app} values, lower lives are predicted for the higher normal load and the lives are predicted to converge with reducing δ_{app} values, giving predicted lives effectively independent of normal load at δ_{app} values of between 1 and 1.5 μm , for Figure 17.

A sensitivity study on the effects of crystallographic orientations has established that the present CP predicted trends for fretting crack nucleation life are independent of crystallographic orientations. An extensive investigation of the effects of grain size and orientation, including realistic distributions, will be addressed in a future study.

The present work has highlighted the important role of frictionally-induced plasticity in fretting crack nucleation. While a COF value of 0.8 has been adopted here, as a realistic steady-state value for fretting of steel, it is clear that this is not a universal value. Hence, further work should also investigate the effects of COF variation on plasticity and associated fretting crack nucleation.

4 Conclusions

The key conclusions from the present study are as follows:

1. A previously-published method for microstructure sensitive fatigue crack initiation prediction is successfully applied to 316L stainless steel to (i) identify the critical microstructural accumulated slip for crack initiation and (ii) predict the low-cycle fatigue behaviour.
2. Finite element modelling of a fretting wear cylinder-on-flat configuration for stainless steel has demonstrated the key role of frictionally-induced cyclic plasticity in fretting, for both a J_2 continuum and a crystal plasticity model, for normal loads lower and higher than the (normal) yield load. The key effects predicted are a significant increase in contact width within the first 12 cycles and an associated significant reduction in peak contact pressure.
3. Compared to J_2 , the CP fretting model predicts (i) more fluctuating distributions of fretting and fatigue variables across the contact, due to material inhomogeneity (random crystallographic orientation), and (ii) significantly larger effects of plasticity on contact width and contact pressure.
4. A microstructure-sensitive crack nucleation methodology for fretting is presented, based on a combination of (i) CP unit cell identification of CP material constants, via comparison with aggregate (bulk material) cyclic stress-strain response, (ii) the identified critical microstructural accumulated slip for crack initiation, and (iii) an FE CP model of fretting under specified loading conditions and tribological data (COF), for identification of critical microstructural location (grain) and value of accumulated plastic slip, and hence crack nucleation life.
5. Application of the latter methodology to fretting crack nucleation prediction for 316L stainless steel for two different normal loads and across a range of applied displacements, spanning across partial slip and gross slip conditions, has demonstrated trends consistent with those of a previously-validated critical-plane SWT (total life) approach and thence with widely accepted trends.
6. The predicted numbers of cycles to initiation were found to be less than 10^4 for the low normal load ($P = 0.5P_y$) and less than 3×10^4 for the higher normal load ($P = 2P_y$). In the $0.5P_y$ case these were between 0.4% and 1.4% of the corresponding CP predicted (SWT) total lives of between 3.1×10^5 and 2.8×10^6 , while in the $2P_y$ case these were between 1% and 11% of the predicted total lives, consistent with previously published fretting data.
7. The proposed fretting crack initiation method is consistent with the length-scales associated with fretting-induced cracks, which is of the order of the grain size, and thus

can be used to study the effects of material inhomogeneities for this length-scale, e.g. crystallographic orientation.

8. The predicted CP distributions of accumulated plastic slip can be used to distinguish between, and hence unify prediction of, wear and fatigue crack initiation. Specifically, in the present work, the gross slip distributions of plastic slip exhibit patterns consistent with wear, i.e. no clear preferred direction and a reasonably uniform distribution over a region similar in size to typical fretting wear scars, whereas the partial slip distributions show patterns consistent with crack nucleation, i.e. localised distributions of plastic slip and a discrete directionality consistent with the experimentally-observed angles of typical (partial slip) fretting cracks.

5 Acknowledgement

The authors wish to acknowledge the SFI/HEA Irish Centre for High-End Computing (ICHEC) for the provision of computational facilities and support. The authors would also like to thank Prof P E McHugh for helpful discussions.

6 References

- [1] Mohd Tobi, A. L., Ding, J., Bandak, G., Leen, S. B., Shipway, P. H., "A study on the interaction between fretting wear and cyclic plasticity for Ti-6Al-4V", *Wear*, 267 (2009) 270-282.
- [2] ASTM F 897-02 (2007) "Standard test method for measuring fretting corrosion of osteosynthesis plates and screws", ASTM International, West Conshohocken, PA, 2007.
- [3] McColl, I.R., Ding, J., Leen, S. B., "Finite element simulation and experimental validation of fretting wear", *Wear*, 256 (2004) 1114-1127.
- [4] Madge, J.J., Leen, S.B., McColl, I.R. Shipway, P.H., "Contact-evolution based predictions of fretting fatigue life: Effects of slip amplitude", *Wear*, 262 (2007) 1159-1170.
- [5] Vingsbo, O., Soderberg, D., "On fretting maps", *Wear*, 126(2) (1988) 131-147.
- [6] Madge, J.J., Leen, S.B., Shipway, P. H., "A combined wear and crack nucleation-propagation methodology for fretting fatigue prediction", *Int .J. Fatigue*, 30 (2008) 1509-1528.
- [7] Ding, J., Bandak, G., Leen, S. B., Williams, E.J., Shipway, P. H., "Experimental characterisation and numerical simulation of contact evolution effect on fretting crack nucleation for Ti-6Al-4V", *Tribology Int*, 42 (2009) 1651-1662.
- [8] Khan, A. S. & Huang, S. *Continuum Theory of Plasticity*. Wiley & Sons , New York, 1995.
- [9] McHugh, P. E., and Connolly, P. J., "Micromechanical modelling of ductile crack growth in the binder phase of WC-Co", *Comput. Mater. Sci.* 27(4):423-436, 2003.
- [10] McGarry, J. P., O'Donnell, B. P., McHugh, P. E., O'Cearbhaill, E., "Computational examination of the effect of material inhomogeneity on the necking of stent struts under tensile loading ", *J Appl Mech.* 74 (2007) 978-990.
- [11] Huang, Y. "A user-material subroutine incorporating single crystal plasticity in the ABAQUS finite element program", Harvard University Report, MECH 178,1991.
- [12] Harewood, F.J.,& McHugh, P. E., "Modeling of Size Dependent Failure in Cardiovascular Stent Struts under Tension and Bending", *Ann. Biomed. Eng.* 35(9) (2007) 1539-1553.
- [13] Mc Dowell, D.L., Dunne, F.P.E., "Microstructure-sensitive computational modelling of fatigue crack formation", *Int J of Fatigue*, 32 (2010) 1521-1542.
- [14] Goh, C.-H., Wallace J.M., Neu, R.W., McDowell, D.L., "Polycrystal plasticity simulations of fretting fatigue", *Int J of Fatigue*, 23 (2001) S423-S435.
- [15] Goh, C.-H., Neu, R.W., McDowell, D.L., "Crystallographic plasticity in fretting of Ti-6AL-4V", *Int J of Plasticity*,19 (2003) 1627-1650.
- [16] Zhang, M., McDowell, D.L., Neu, R.W., "Microstructure sensitivity of fretting fatigue based on computational crystal plasticity", *Tribology Int*, 42 (2009) 1286-1296.
- [17] Zhang, M., McDowell, D.L., Neu, R.W., "Microstructure sensitivity modelling: Application to fretting contacts", *Int J of Fatigue*, 31 (2009) 1397-1406.
- [18] Manonukul, A. & Dunne, F. P. E., "High and low cycle fatigue crack initiation using polycrystal plasticity", *Proc. R. Soc. A*, 460 (2004) 1881-1903.

- 1 [19] Pierce, D., Asaro, R.J., Needleman, A., "Material rate dependence and localised deformation in
2 crystalline solids", *Acta Metall. Mater.* 31 (12) (1983) 1951-1976.
- 3 [20] Maeng, Y.W., Kang, Y.H., "Creep-fatigue and fatigue crack growth properties of 316LN
4 stainless steel at high temperature " *Proc. 15th International Conference on Structural Mechanics in
5 Reactor Technology*, Korea, 1999.
- 6 [21] Savage, P., O'Donnell, B. P., McHugh, P. E., Murphy, B. P. and Quinn, D. F., "Coronary stent
7 strut size dependent stress-strain response investigated using micromechanical finite element
8 models", *Ann. Biomed. Eng.* 32(2):202-211, 2004.
- 9 [22] Lemaitre, J. & Chaboche, J.-L. *Mechanics of Solid Materials*, Cambridge University Press,
10 Cambridge, 1990.
- 11 [23] Socie, D., "Multiaxial fatigue damage models" *J Eng Mater Technol*, 109 (1987) 293-299.
- 12 [24] Sum, W.S., Williams, E.J., Leen, S.B., "Finite element critical plane, fatigue life prediction of
13 simple and complex contact configurations", *Int .J. Fatigue*, 27 (2005) 403-416.
- 14 [25] Houghton, D., Wavish, P.M., Williams, E.J., Leen, S.B., "Multiaxial fretting fatigue testing and
15 prediction for splined couplings " *Int .J. Fatigue*, 31 (2009) 1805-1815.
- 16 [26] Ambrico, J.M., Begley, M.R., "Plasticity in fretting contact", *J Mech Phys Solids*, 48 (2000)
17 2391-2417.
- 18 [27] Johnson, K.L., *Contact Mechanics*, Cambridge University Press, Cambridge, 1985.
- 19 [28] Golden, P.J., Calcaterra, J.R., "A fracture mechanics life prediction methodology applied to
20 dovetail fretting", *Tribology Int*, 39 (2009) 1172-1180.
- 21 [29] Zhou, Z., R., Vincent., L., "Mixed fretting regime", *Wear*, 188-183 (1995) 531-536
- 22 [30] Nakazawa, K., Maruyama, N., Hanawa. T., "Effect of contact pressure on fretting fatigue of
23 austenitic stainless steel", *Tribology Int*, 36 (2003) 79-85.
- 24
25
26
27
28
29
30
31
32
33
34
35
36
37
38
39
40
41
42
43
44
45
46
47
48
49
50
51
52
53
54
55
56
57
58
59
60
61
62
63
64
65

Table 1. Material constants, including non-linear kinematic hardening data, for 316L SS [22].

E	209 GPa
ν	0.28
k	300 MPa
C	30000 MPa
γ	60

Table 2. Identified CP constitutive constants for cyclic behaviour of 316L SS

h_0	60 MPa
g_∞	250 MPa
g_0	70 MPa
\dot{a}	0.001s^{-1}
n	20

Table 3. Fatigue constants for Smith-Watson-Topper equation for 316L SS [22].

σ'_f	3280 MPa
ε'_f	0.34
b	-0.175
c	-0.483

Table 4. J_2 -predicted slip regimes and contact width a_f/a_o ratios across a range of δ_{app} , where a_f is final contact width (after 12 cycles).

δ_{app} (μm)	$P/P_y = 0.5$		$P/P_y = 2$	
	Slip regime	a_f/a_o	Slip regime	a_f/a_o
0.5	Partial slip	1	Partial slip	1.072
0.75	Partial slip	1.25	Partial slip	1.138
1	Gross slip	1.25	Partial slip	1.138
1.25	Gross slip	1.25	Partial slip	1.205
1.5	Gross slip	1.25	Partial slip	1.206
2	Gross slip	1.25	Partial slip	1.407

Note: $a_o = 0.052$ mm for $P/P_y = 0.5$;

$a_o = 0.097$ mm for $P/P_y = 2$.

Table 5. CP-predicted slip regimes and contact width a_f/a_o ratios across a range of δ_{app} , where a_f is final contact width (after 12 cycles).

δ_{app} (μm)	$P/P_y = 0.5$		$P/P_y = 2$	
	Slip regime	a_f/a_o	Slip regime	a_f/a_o
0.5	Partial slip	1.376	Partial slip	1.292
0.75	Partial slip	1.690	Partial slip	1.344
1	Gross slip	1.879	Partial slip	1.424
1.25	Gross slip	1.880	Partial slip	1.504
1.5	Gross slip	1.942	Partial slip	1.612
2	Gross slip	1.882	Partial slip	1.830

Note: $a_o = 0.052$ mm for $P/P_y = 0.5$;

$a_o = 0.123$ mm for $P/P_y = 2$.

Table 6. J_2 -predicted position and angle of maximum critical plane SWT value along the substrate surface for different displacement amplitudes for $P/P_y = 0.5$.

δ_{app} (μm)	SWT (MPa)	Failure location, x/a_0	Life	Angle
0.5	0.340	-0.818	1446630	165°
0.75	0.427	0.769	828854	160°
1	0.656	0.962	301880	165°
1.25	0.648	0.962	309436	165°
1.5	0.668	-0.943	288482	15°
2	0.684	-0.943	274759	160°

Table 7. J_2 -predicted position and angle of maximum critical plane SWT value along the substrate surface for different displacement amplitudes for $P/P_y = 2$.

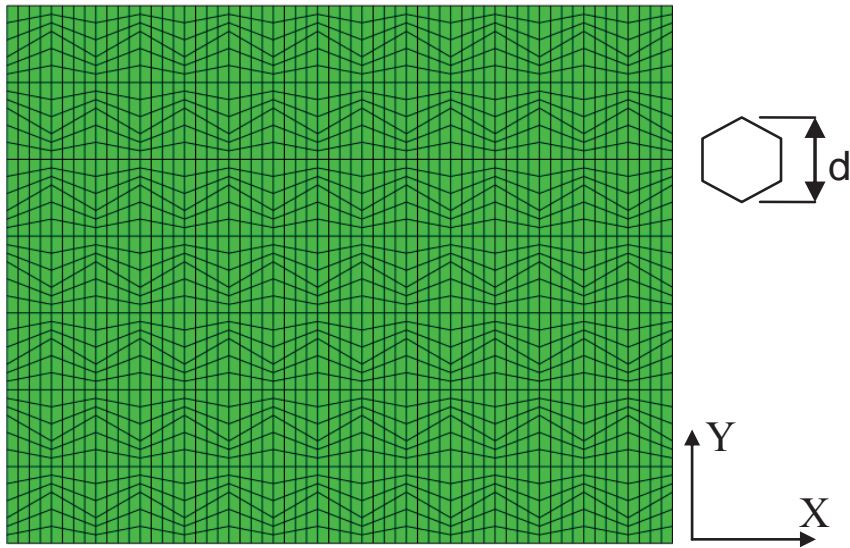
δ_{app} (μm)	SWT (MPa)	Failure location, x/a_0	Life	Angle
0.5	0.291	1.039	2125853	160°
0.75	0.394	1.039	1013391	15°
1	0.585	-1.037	393459	15°
1.25	0.697	-1.104	262274	15°
1.5	0.842	-1.171	170617	15°
2	1.473	-1.324	50087	160°

Table 8. CP-predicted crack initiation life, N_i , location and angle for a range of displacement amplitudes for $P/P_y = 0.5$ based on p_{crit} .

δ_{app} (μm)	p_{cyc}	Position x/a_0	N_i	Angle
0.5	0.0074	1.058	7946	N/A
0.75	0.011	1.347	5345	N/A
1	0.0115	1.443	5113	N/A
1.25	0.012	1.539	4900	N/A
1.5	0.012	1.539	4900	N/A
2	0.0125	1.539	4704	N/A

Table 9. CP-predicted crack initiation life, N_i , location and angle for a range of displacement amplitudes for $P/P_y = 2$, based on p_{crit} .

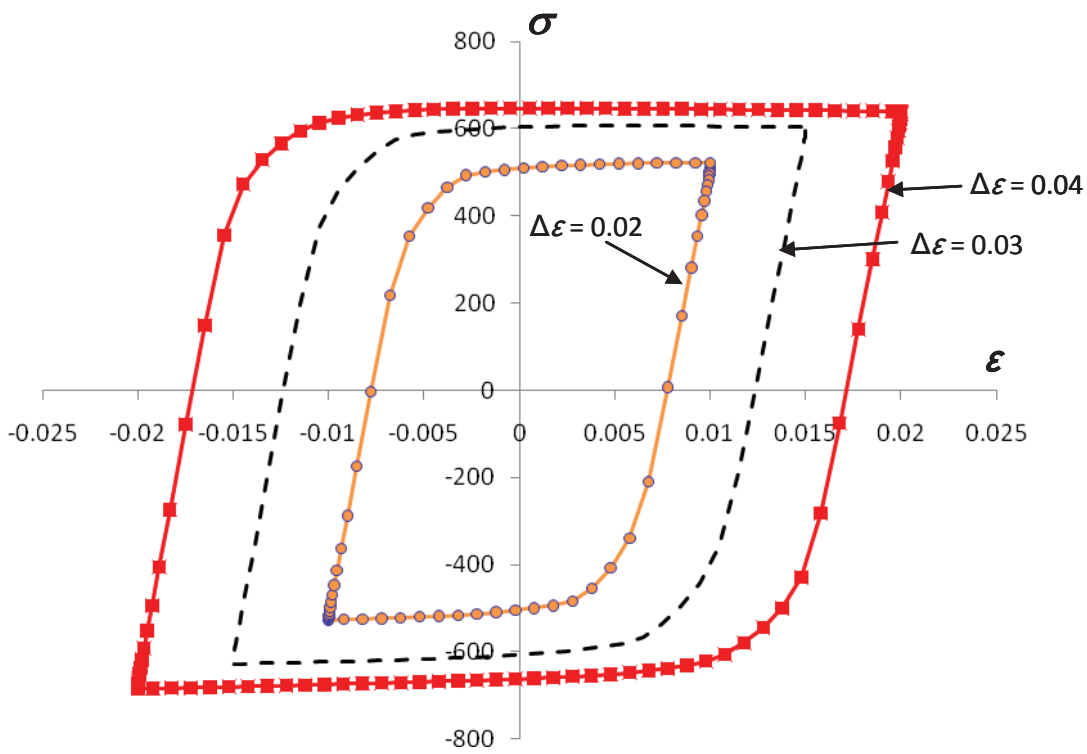
δ_{app} (μm)	p_{cyc}	Position x/a_0	N_i	Angle
0.5	0.0022	-1.174	26727	52.9°
0.75	0.0050	-1.292	11879	51.5°
1	0.0084	-1.344	7000	50°
1.25	0.0090	1.377	6497	48.7°
1.5	0.0159	-1.555	3709	N/A
2	0.0169	-1.826	3469	N/A



1

2 Figure 1. Plane strain unit cell FE model for crystal plasticity uniaxial simulations of 316L stainless
3 steel; inset shows assumed (regular) hexagonal grain shape and grain size dimension, d .

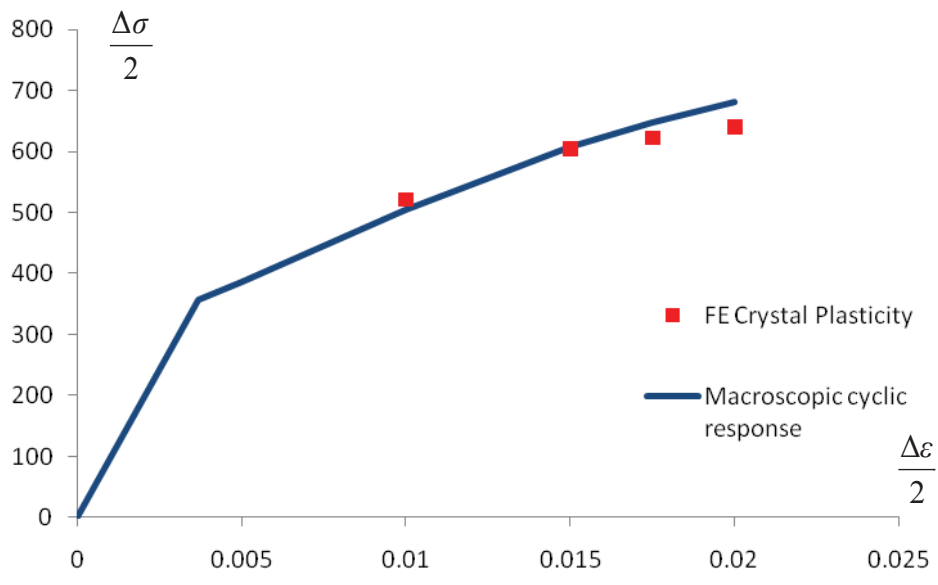
4



5

6 Figure 2. CP predicted stabilised hysteresis loops for 316L SS

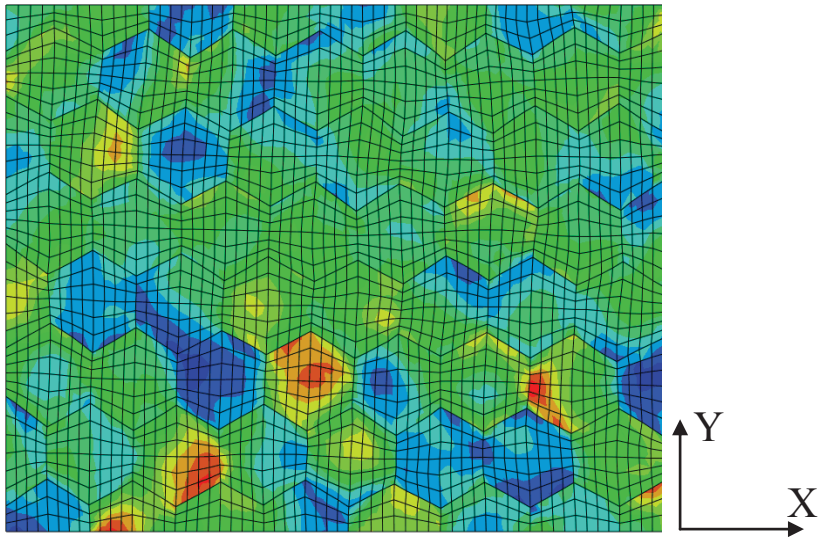
7



1

2 Figure 3. Comparison of CP cyclic stress-strain curve with macroscopic (aggregate) cyclic stress-
 3 strain curve for 316L stainless steel, as represented by data in Table 1 [22].

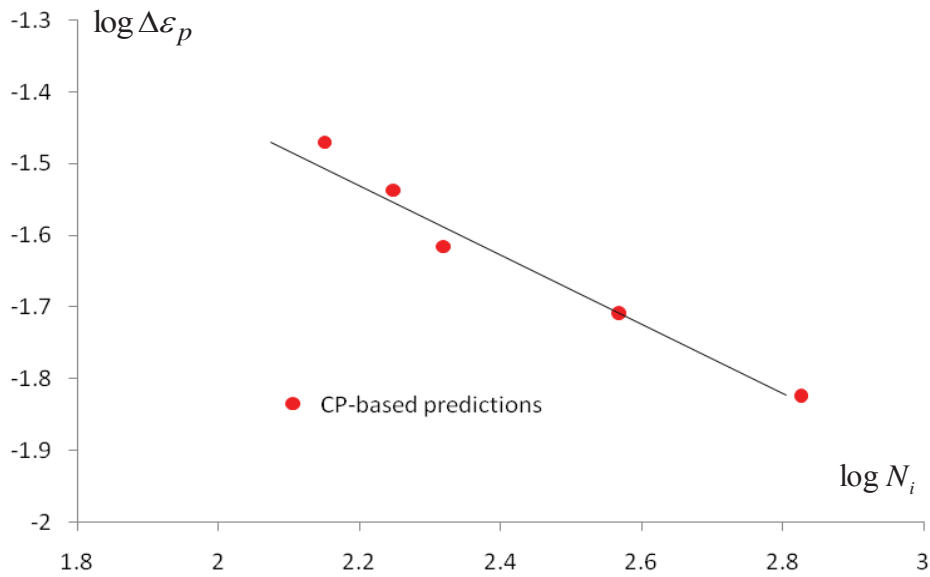
4



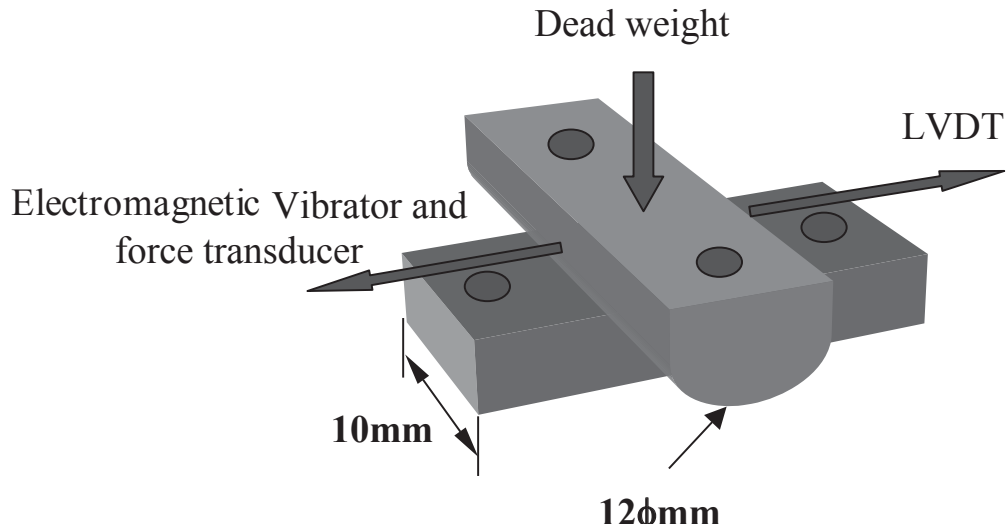
5

6 Figure 4. FE predicted inhomogeneous distribution of p for $\Delta \varepsilon = 2\%$.

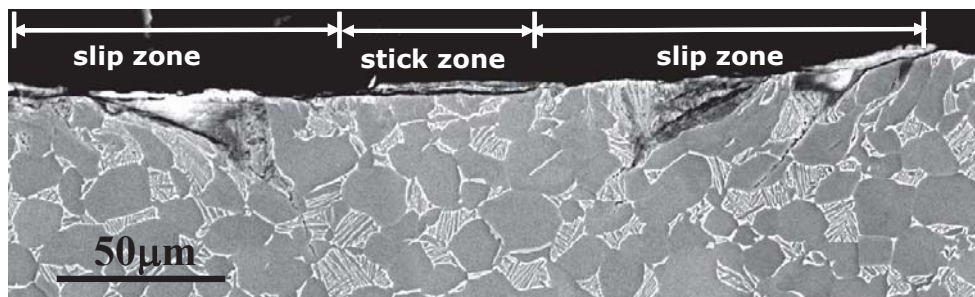
7



1
 2 Figure 5. Validation of identified p_{crit} value for crack initiation in 316L stainless steel, based on CP
 3 unit cell predictions, against measured Coffin-Manson relationship.

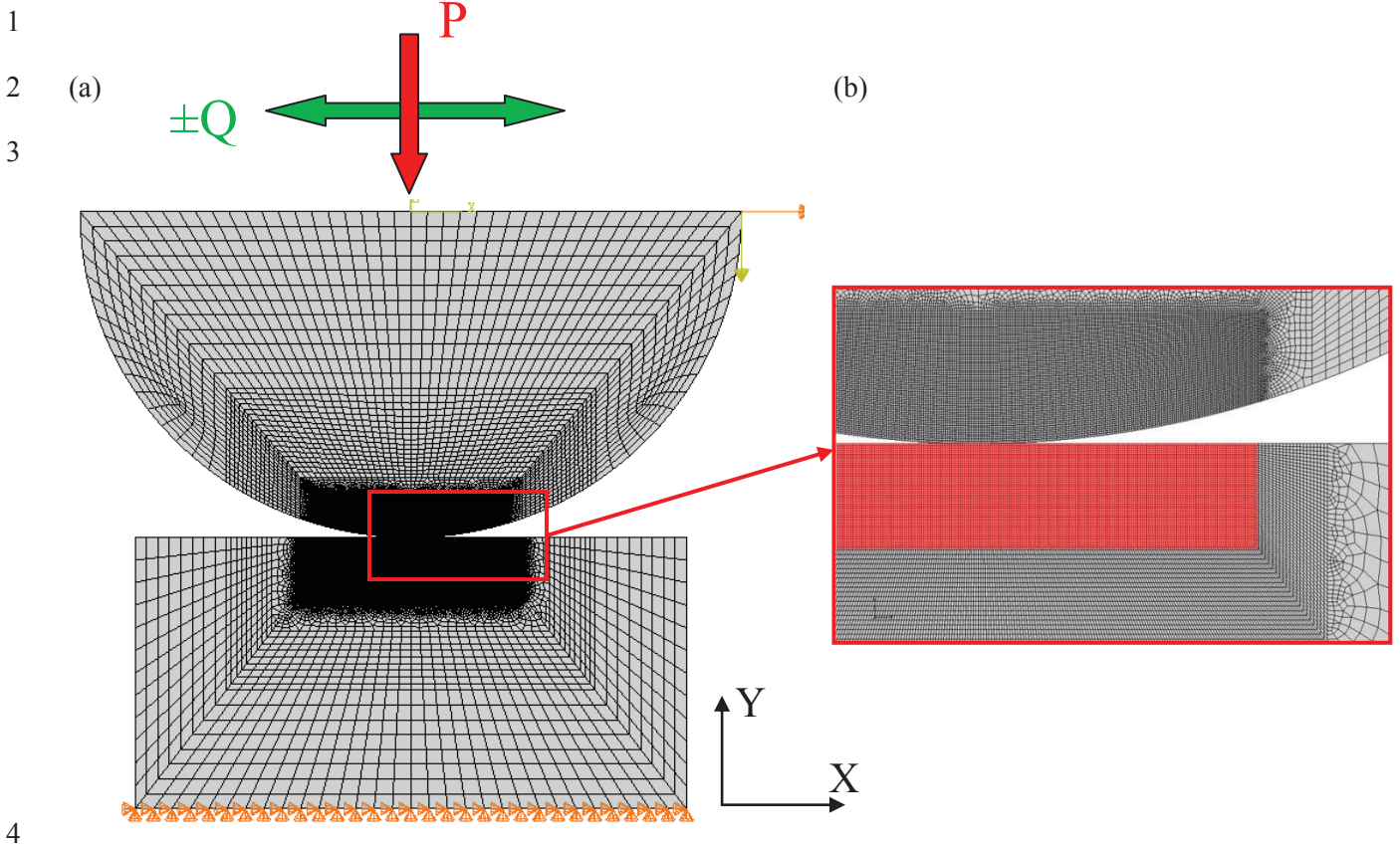


4
 5 Figure 6. Schematic of University of Nottingham round-on-flat fretting wear arrangement [7].

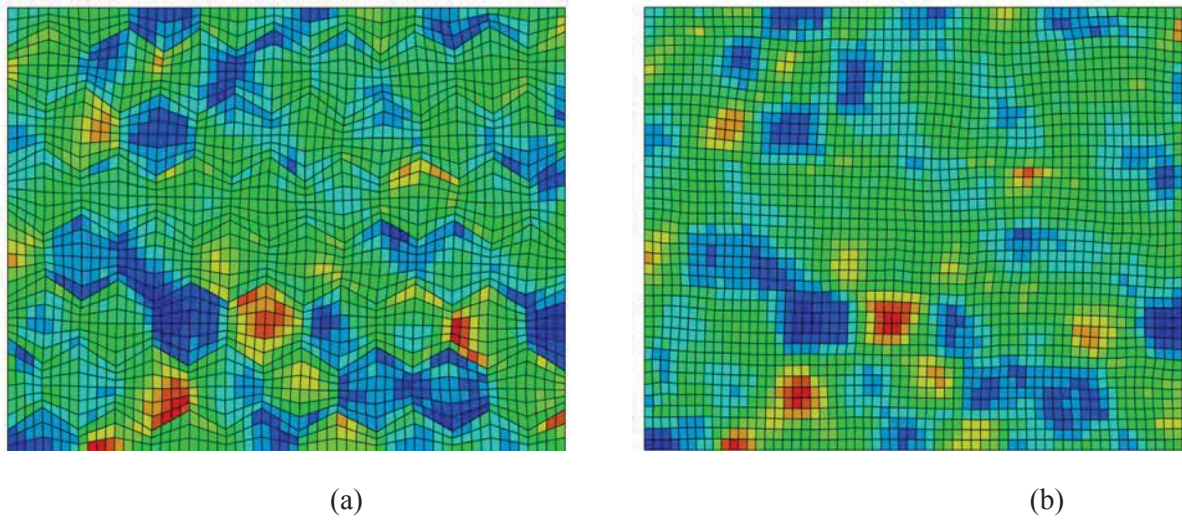


6
 7 Figure 7. SEM images of partial slip crack initiation in Ti6Al4V [7], after 300,000 cycles under a
 8 normal load of 100 N/mm and a 50 μm stroke.

9

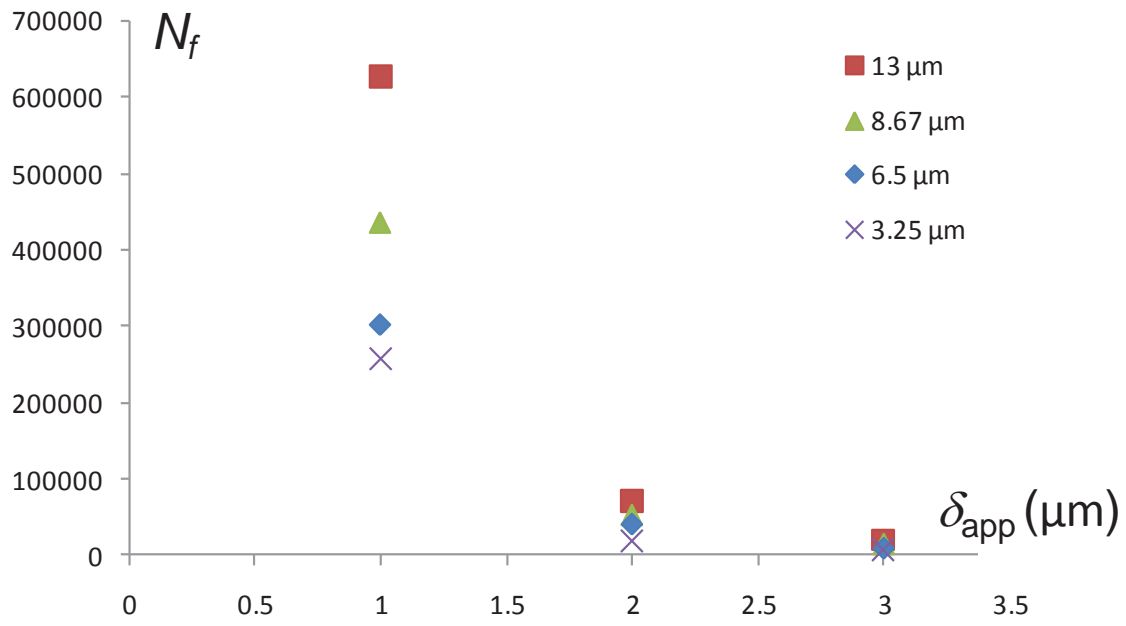


5 Figure 8. (a) Boundary conditions, loads, and displacements in the fretting model; (b) detail from the
6 crystal plasticity region in the model.



11 Figure 9. Comparison of CP predicted cyclic plasticity response under applied strain range, $\Delta\varepsilon$, of 2%
12 for (a) hexagonal grain (deformed) mesh and (b) matching square grain (deformed) mesh; both grain
13 morphologies predict almost identical maximum values of accumulated plastic slip of $p \approx 1.79$.

15



1

2 Figure 10. The effect of mesh refinement on predicted total life (N_f) as a function of applied
 3 displacement (the legend indicates square element side lengths).

4

5

6

7

8

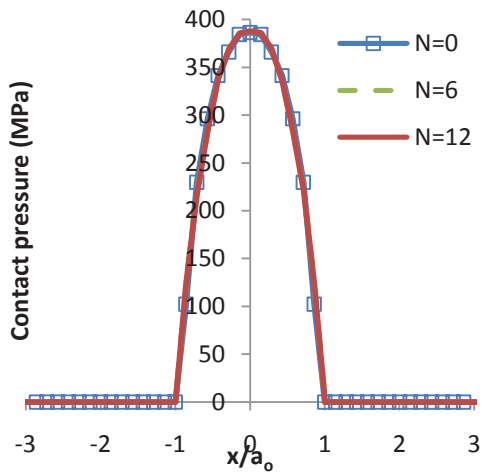
9

10

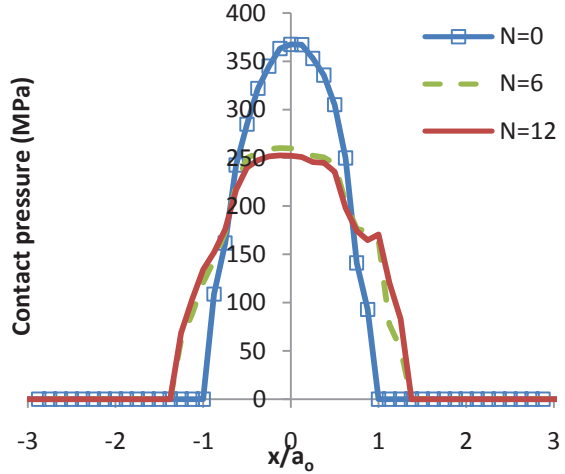
11

12

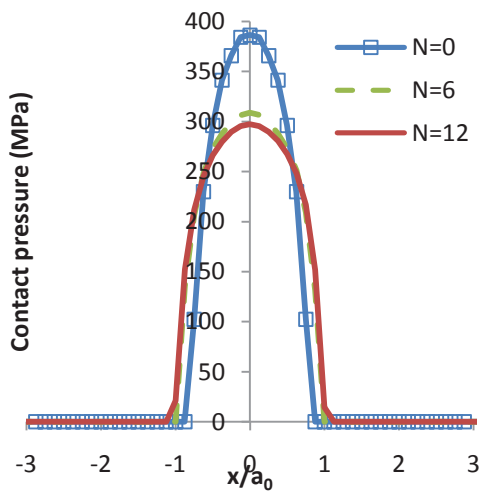
13



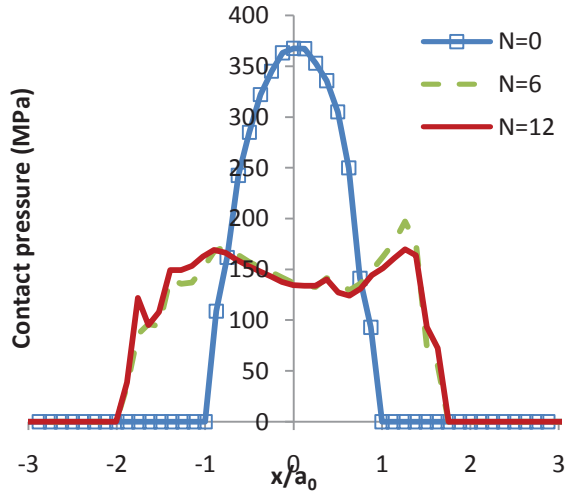
(a) J_2 model, $\delta_{app} = 0.5 \mu\text{m}$



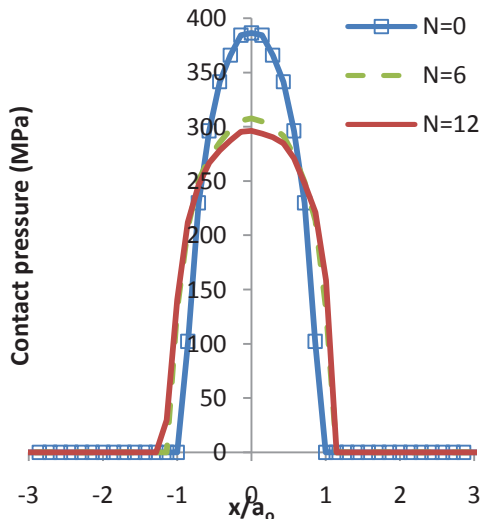
(b) CP model, $\delta_{app} = 0.5 \mu\text{m}$



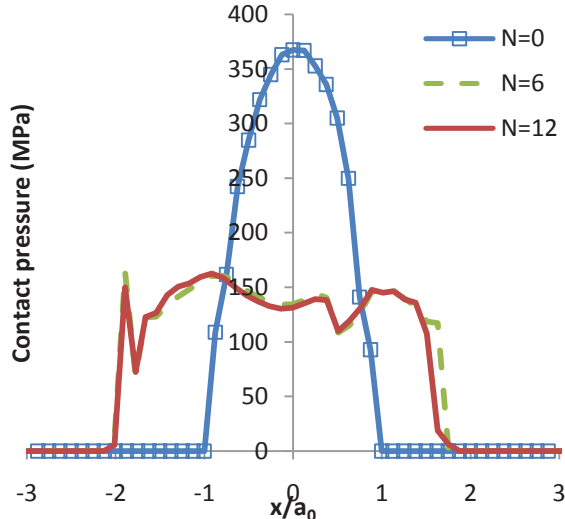
(c) J_2 model, $\delta_{app} = 1 \mu\text{m}$



(d) CP model, $\delta_{app} = 1 \mu\text{m}$

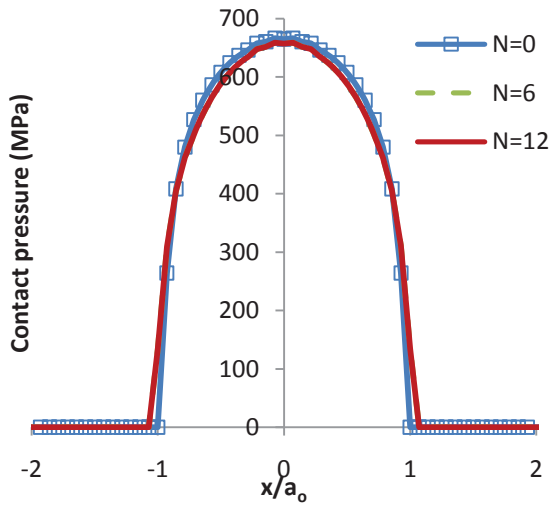


(e) J_2 model, $\delta_{app} = 2 \mu\text{m}$

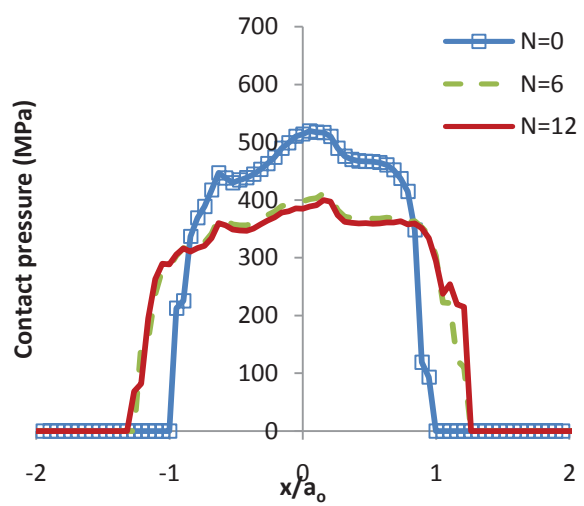


(f) CP model, $\delta_{app} = 2 \mu\text{m}$

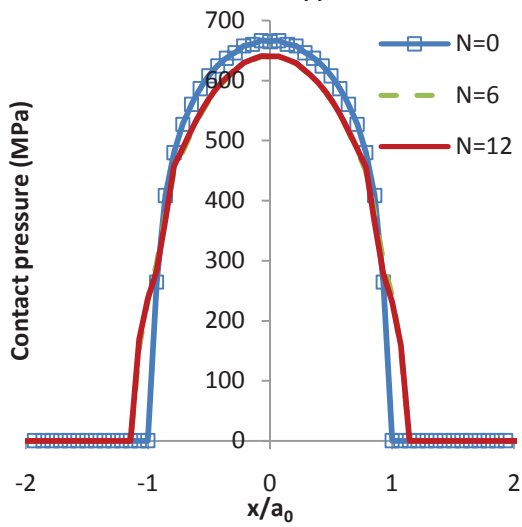
Figure 11. J_2 and CP fretting model predicted evolutions of contact pressure under different tangential displacements (δ_{app}) for $P/P_y = 0.5$.



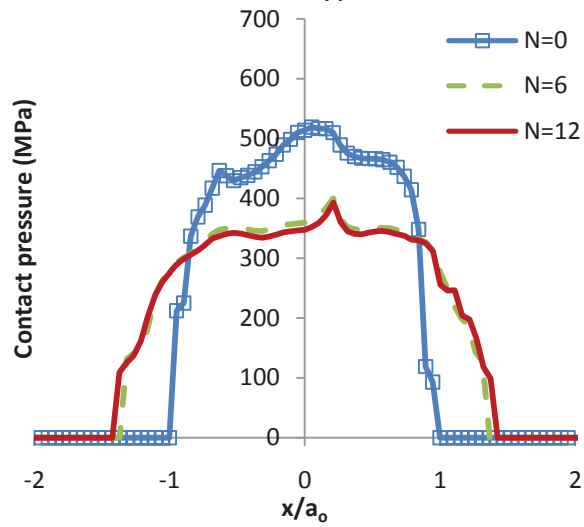
(a) J_2 model, $\delta_{app} = 0.5 \mu\text{m}$



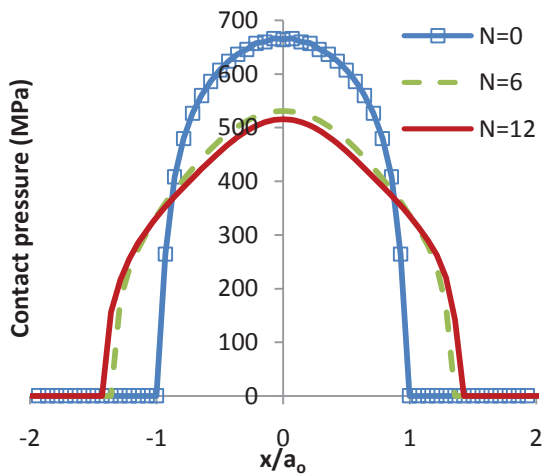
(b) CP model, $\delta_{app} = 0.5 \mu\text{m}$



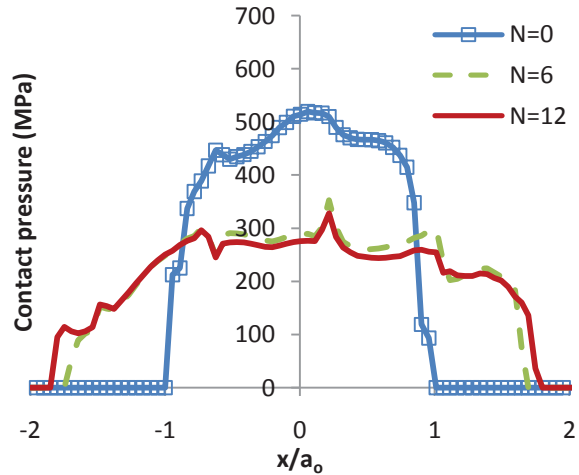
(c) J_2 model, $\delta_{app} = 1 \mu\text{m}$



(d) CP model, $\delta_{app} = 1 \mu\text{m}$

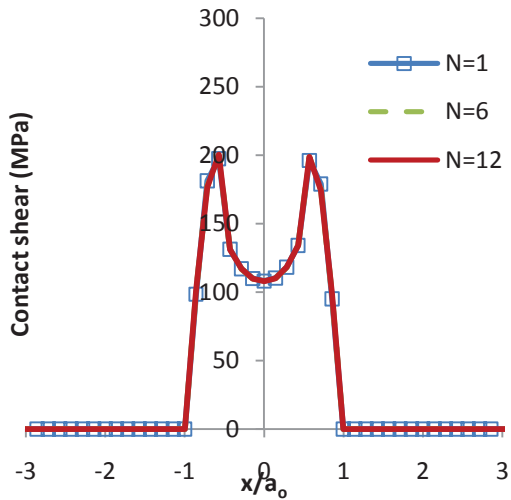


(e) J_2 model, $\delta_{app} = 2 \mu\text{m}$

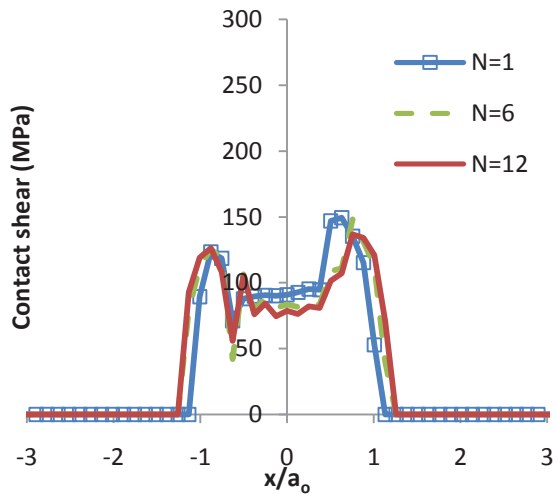


(f) CP model, $\delta_{app} = 2 \mu\text{m}$

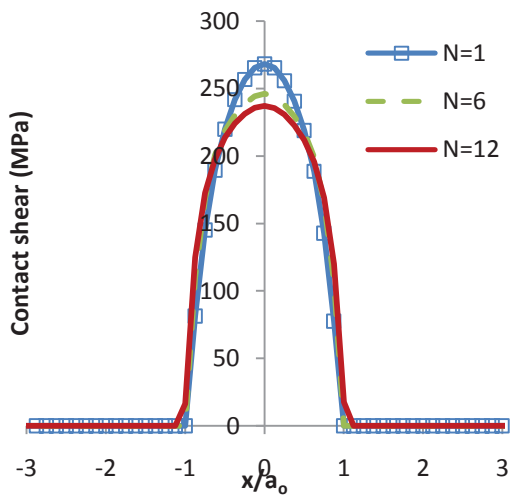
Figure 12. J_2 and CP fretting model predicted evolutions of contact pressure under different tangential displacements (δ_{app}) for $P/P_y = 2$.



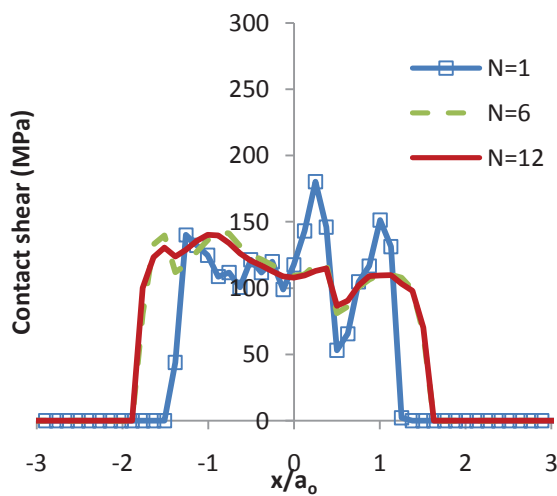
(a) J_2 model, $\delta_{app} = 0.5 \mu\text{m}$



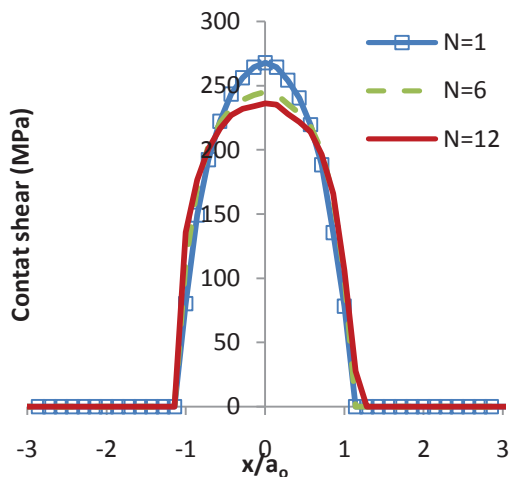
(b) CP model, $\delta_{app} = 0.5 \mu\text{m}$



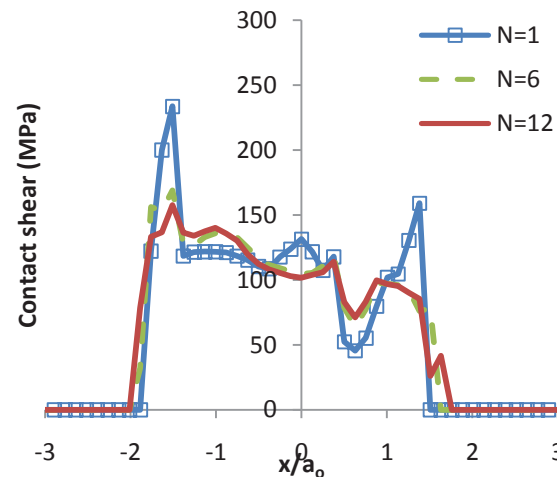
(c) J_2 model, $\delta_{app} = 1 \mu\text{m}$



(d) CP model, $\delta_{app} = 1 \mu\text{m}$

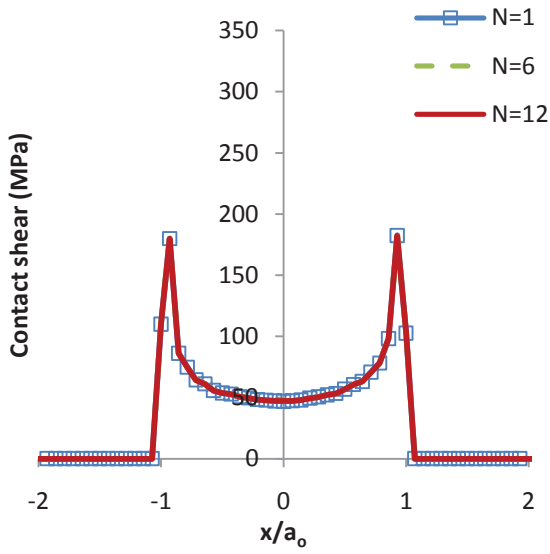


(e) J_2 model, $\delta_{app} = 2 \mu\text{m}$

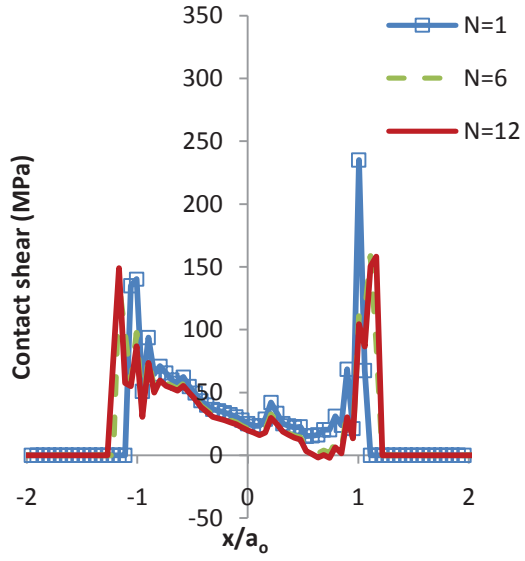


(f) CP model, $\delta_{app} = 2 \mu\text{m}$

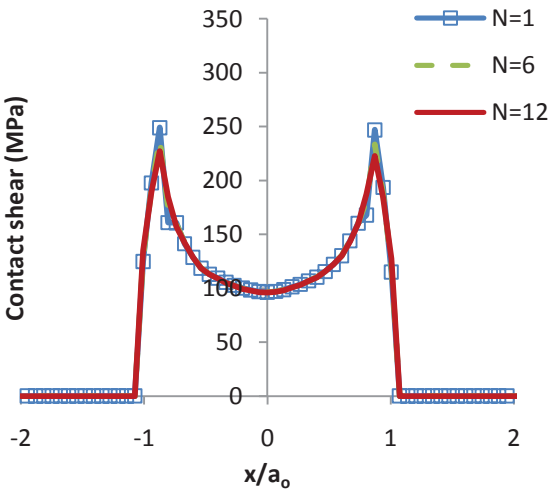
Figure 13. J_2 and CP fretting model predicted evolutions of contact shear traction under different tangential displacements (δ_{app}) for $P/P_y = 0.5$.



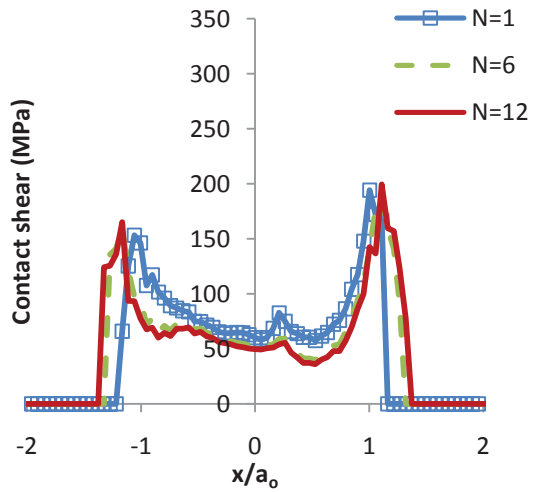
(a) J_2 model, $\delta_{app} = 0.5 \mu\text{m}$



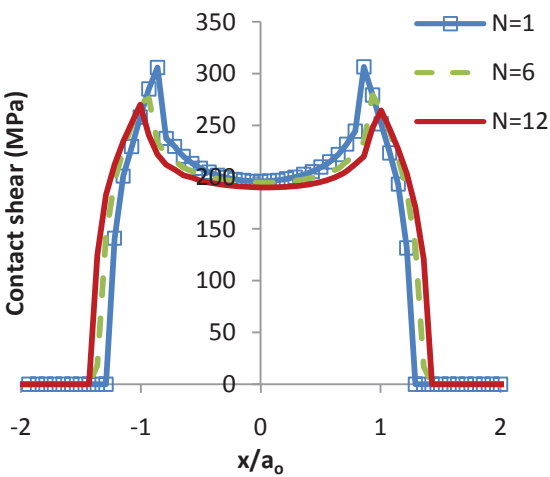
(b) CP model, $\delta_{app} = 0.5 \mu\text{m}$



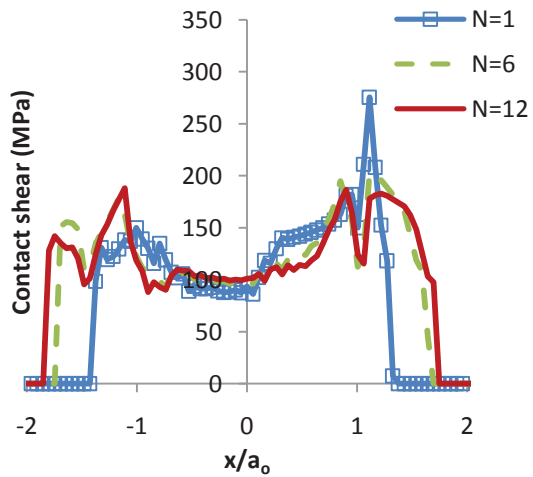
(c) J_2 model, $\delta_{app} = 1 \mu\text{m}$



(d) CP model, $\delta_{app} = 1 \mu\text{m}$

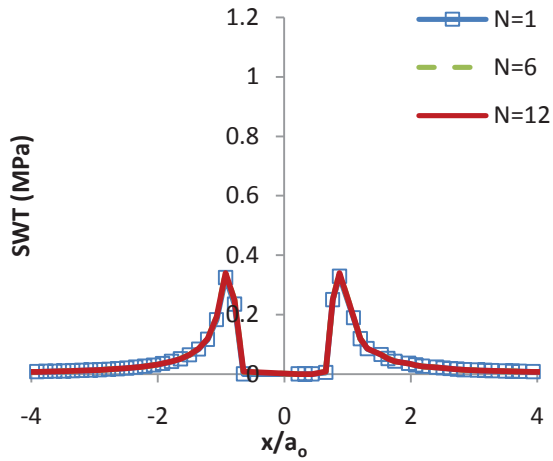


(e) J_2 model, $\delta_{app} = 2 \mu\text{m}$

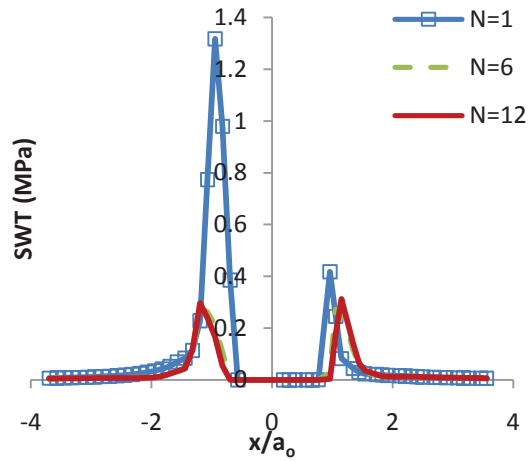


(f) CP model, $\delta_{app} = 2 \mu\text{m}$

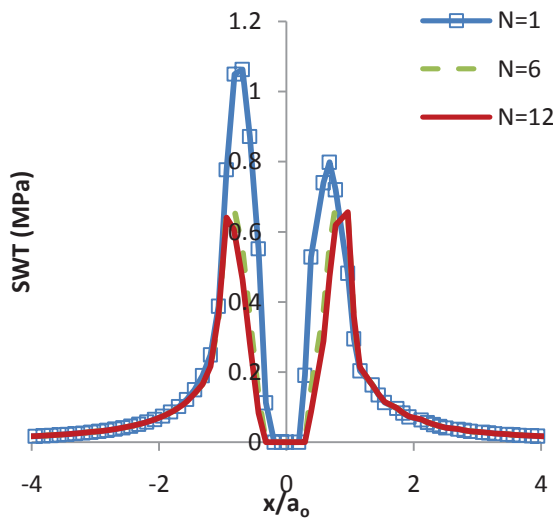
Figure 14. J_2 and CP fretting model predicted evolutions of contact shear traction under different tangential displacements (δ_{app}) for $P/P_y = 2$.



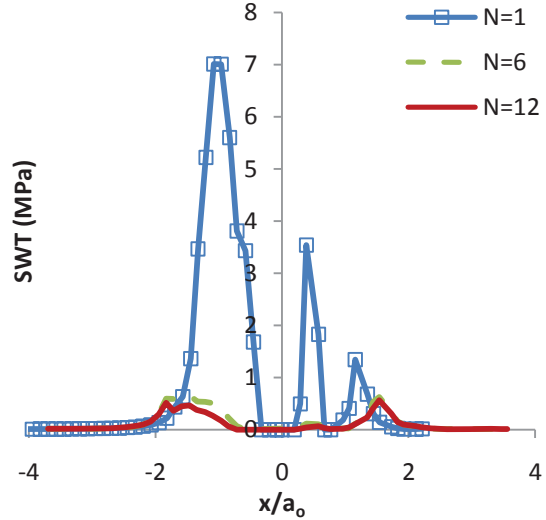
(a) J_2 model, $\delta_{app} = 0.5 \mu\text{m}$



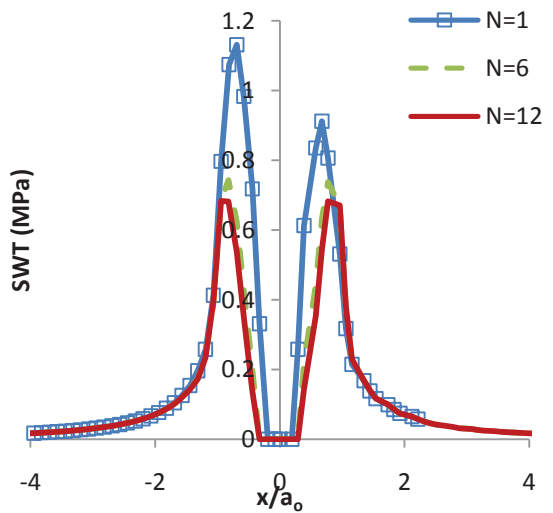
(b) CP model, $\delta_{app} = 0.5 \mu\text{m}$



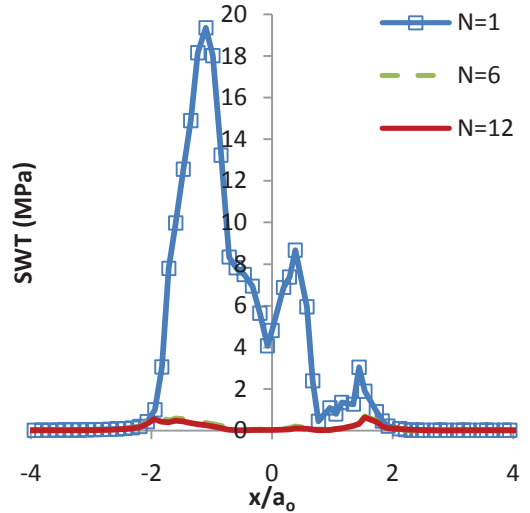
(c) J_2 model, $\delta_{app} = 1 \mu\text{m}$



(d) CP model, $\delta_{app} = 1 \mu\text{m}$

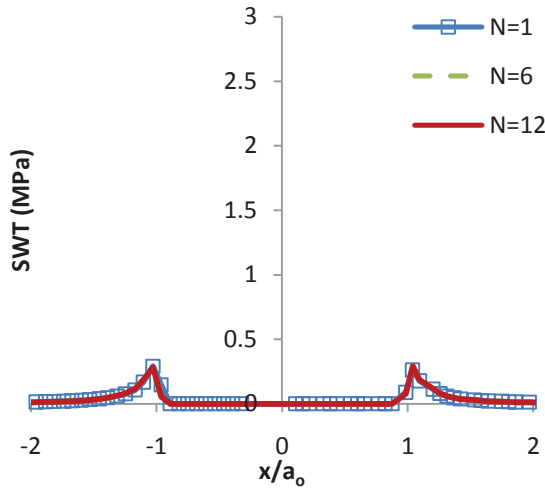


(e) J_2 model, $\delta_{app} = 2 \mu\text{m}$

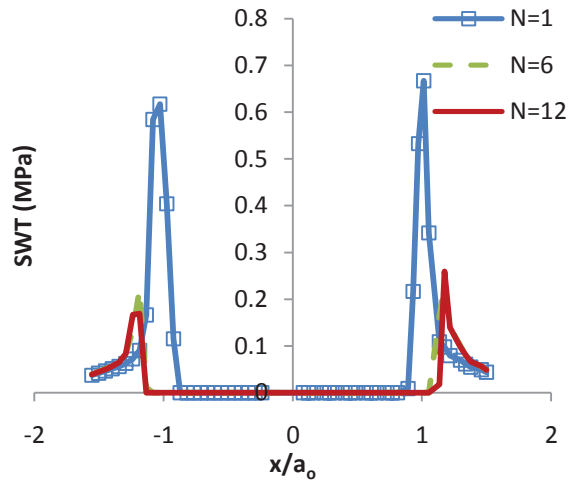


(f) CP model, $\delta_{app} = 2 \mu\text{m}$

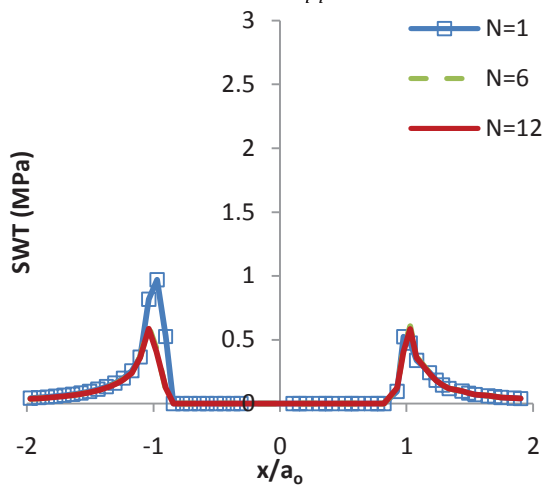
Figure 15. J_2 and CP fretting model predicted evolutions of SWT distribution under different tangential displacements (δ_{app}) for $P/P_y = 0.5$.



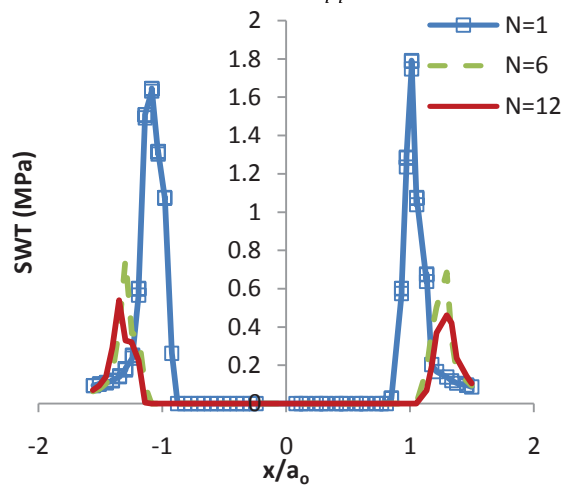
(a) J_2 model, $\delta_{app} = 0.5 \mu\text{m}$



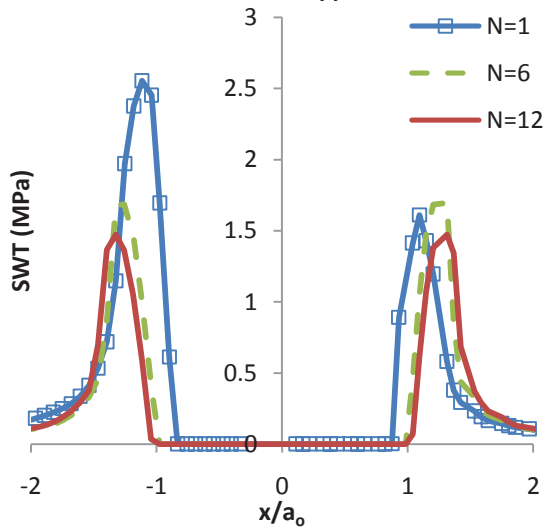
(b) CP model, $\delta_{app} = 0.5 \mu\text{m}$



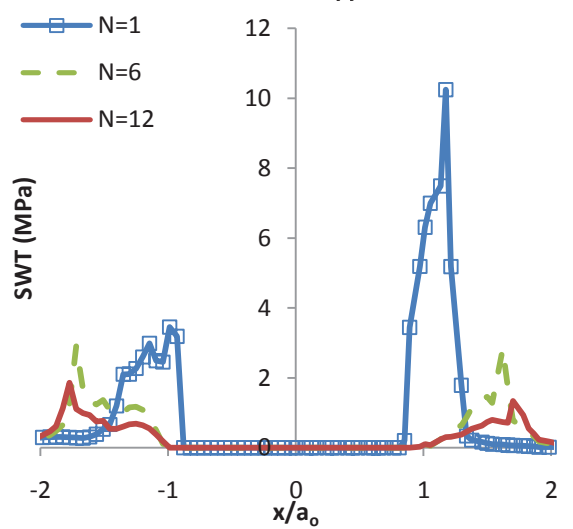
(c) J_2 model, $\delta_{app} = 1 \mu\text{m}$



(d) CP model, $\delta_{app} = 1 \mu\text{m}$

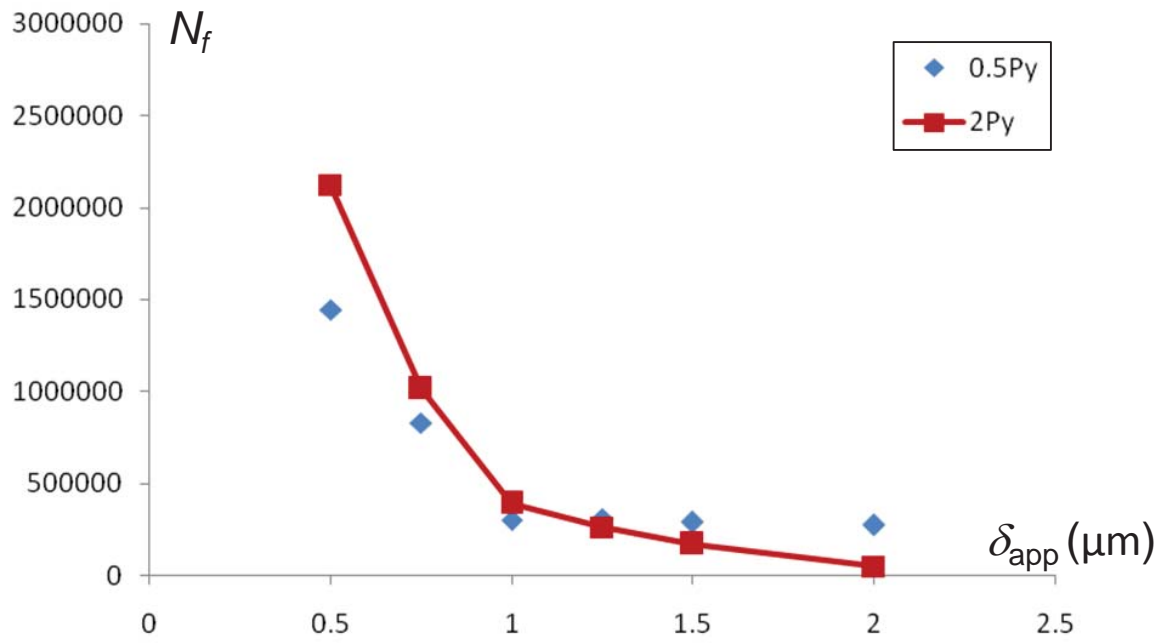


(e) J_2 model, $\delta_{app} = 2 \mu\text{m}$

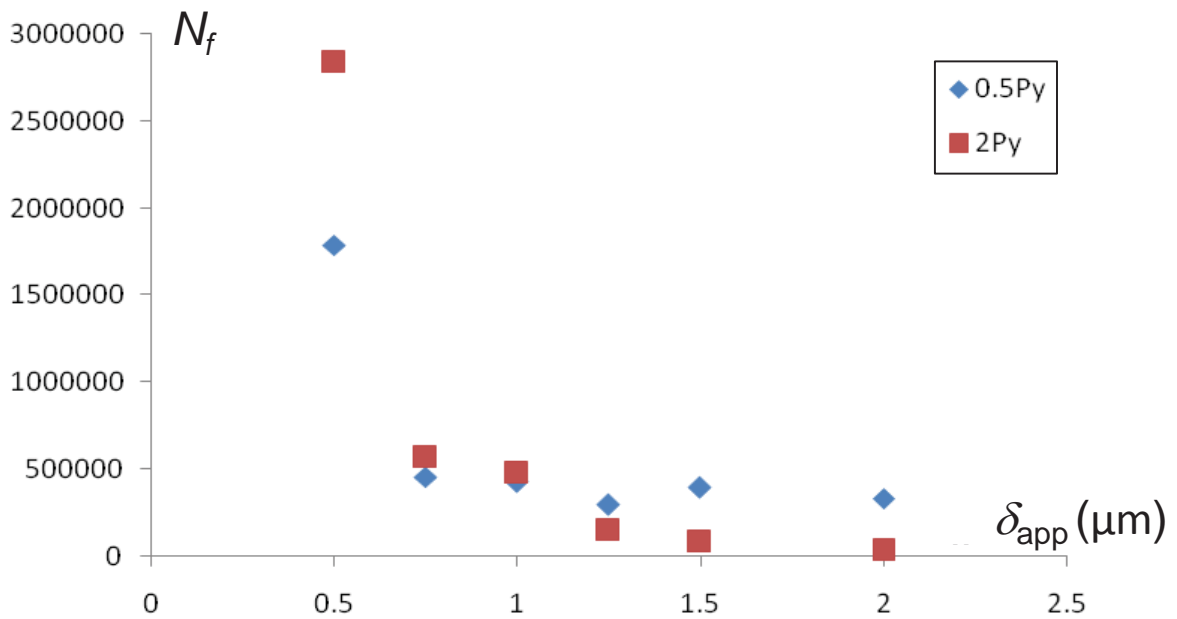


(f) CP model, $\delta_{app} = 2 \mu\text{m}$

Figure 16. J_2 and CP fretting model predicted evolutions of SWT distribution under different tangential displacements (δ_{app}) for $P/P_y = 2$.

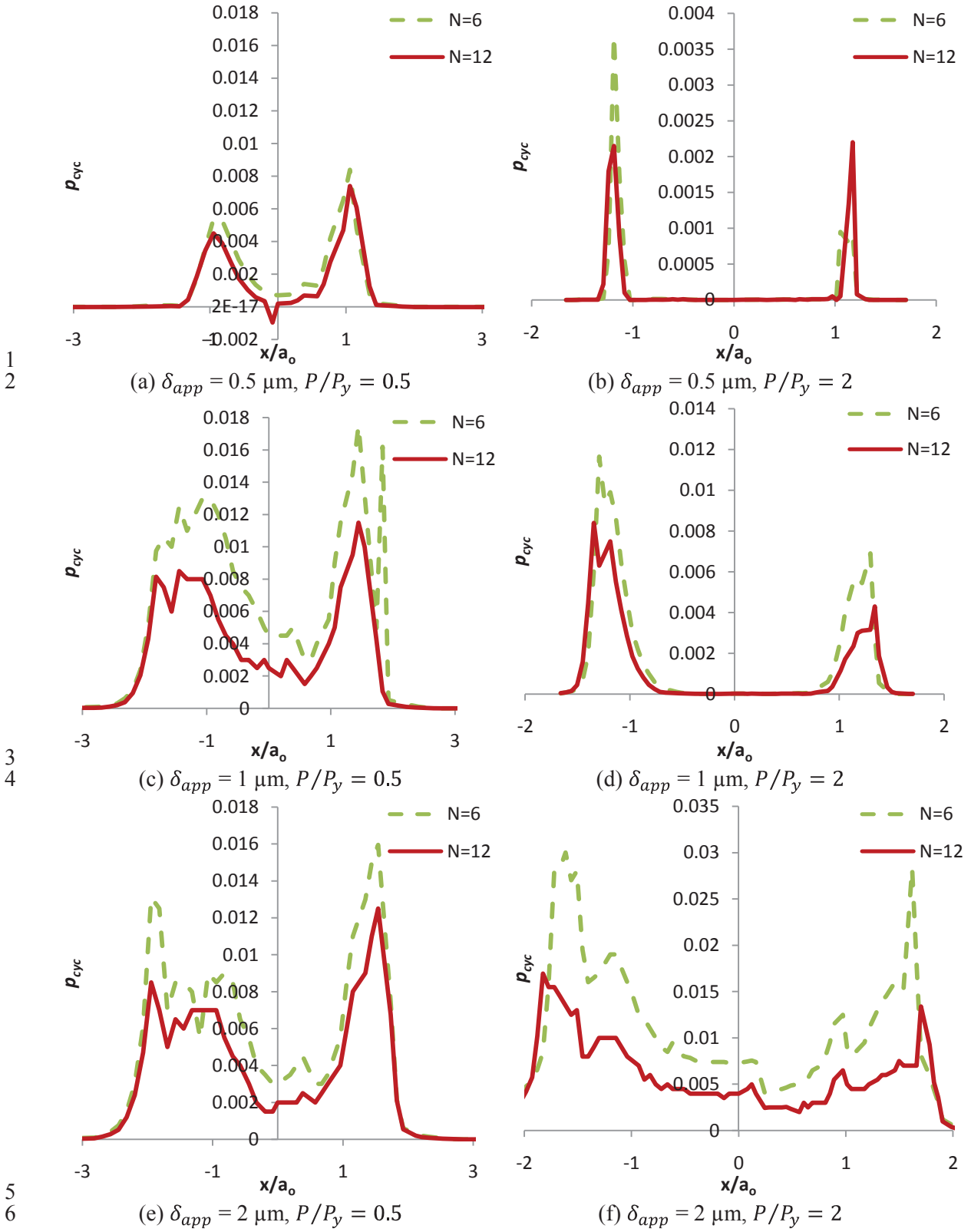


(a)



(b)

Figure 17. SWT-predicted N_f as a function of displacement amplitude for $P/P_y = 2$ and $P/P_y = 0.5$, using (a) J_2 -fretting model and (b) CP fretting model.

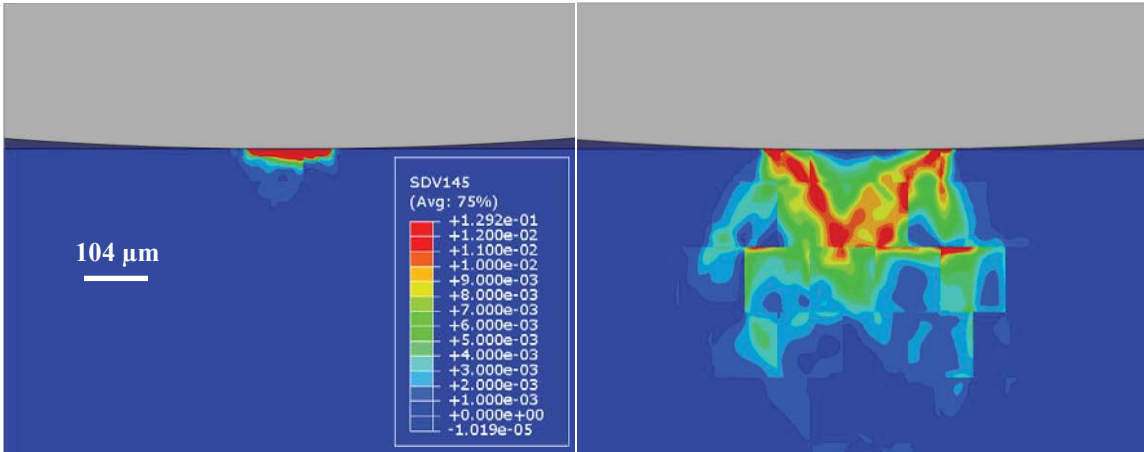


1
2

3
4

5
6
7

8 Figure 18. Predicted evolution of accumulated plastic slip per cycle, p_{cyc} , under different tangential
9 displacements (δ_{app}) and normal loads (P).

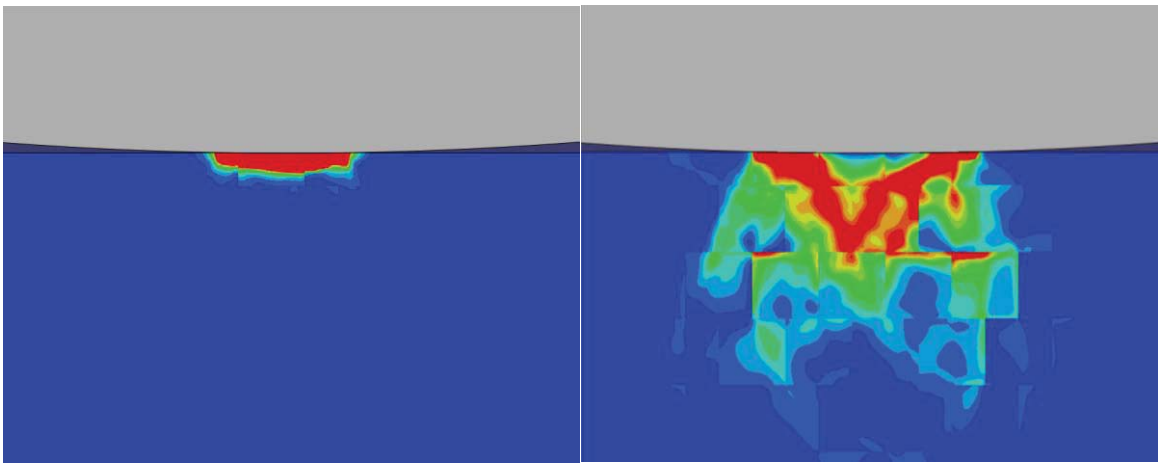


1

2

(a) $\delta_{app} = 0.5 \mu\text{m}$, $P/P_y = 0.5$

(b) $\delta_{app} = 0.5 \mu\text{m}$, $P/P_y = 2$

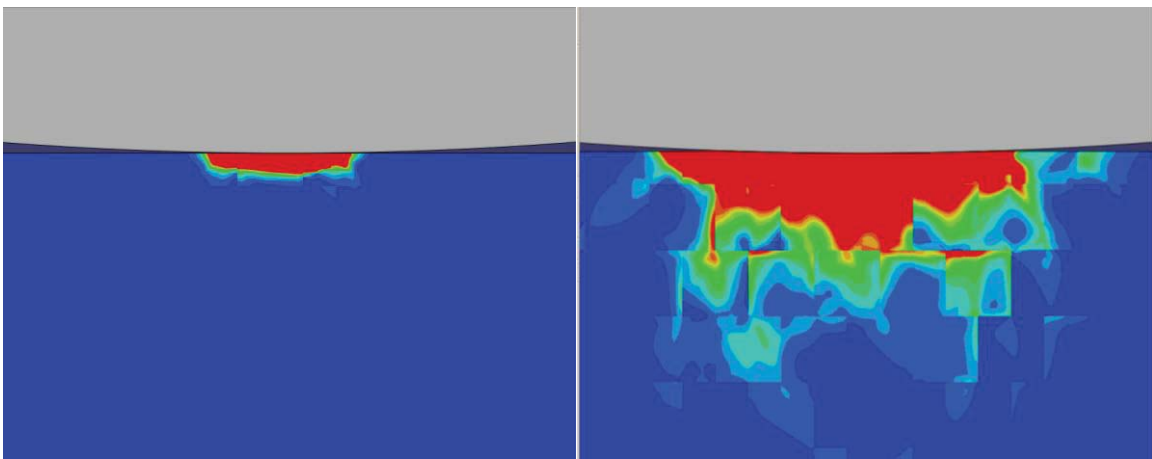


3

4

(c) $\delta_{app} = 1 \mu\text{m}$, $P/P_y = 0.5$

(d) $\delta_{app} = 1 \mu\text{m}$, $P/P_y = 2$



5

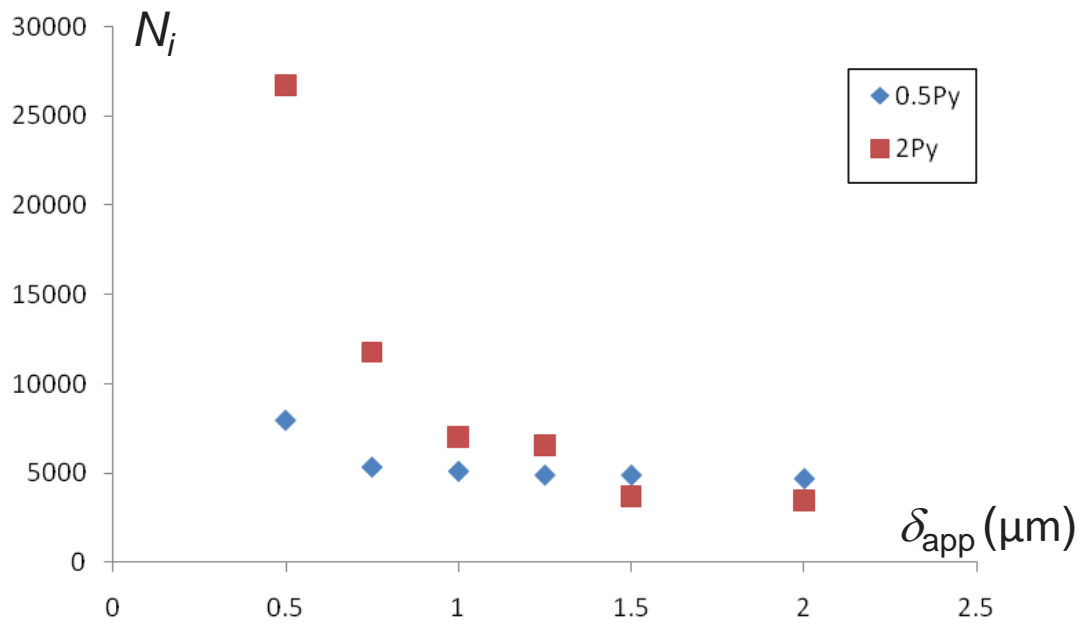
6

(e) $\delta_{app} = 2 \mu\text{m}$, $P/P_y = 0.5$

(f) $\delta_{app} = 2 \mu\text{m}$, $P/P_y = 2$

7 Figure 19. FE predicted contour plots of accumulated plastic slip p under different tangential
8 displacements (δ_{app}) and normal loads.

9



1

2 Figure 20. p_{crit} -predicted initiation life as a function of displacement amplitudes for $P/P_y = 2$ and
 3 $P/P_y = 0.5$.

4

5

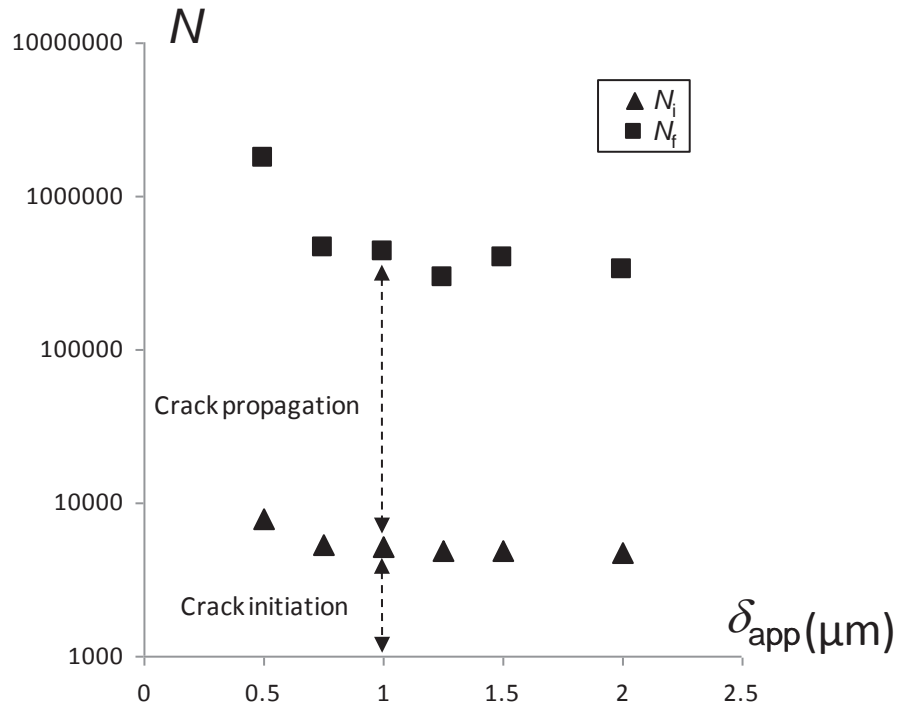
6

7

8

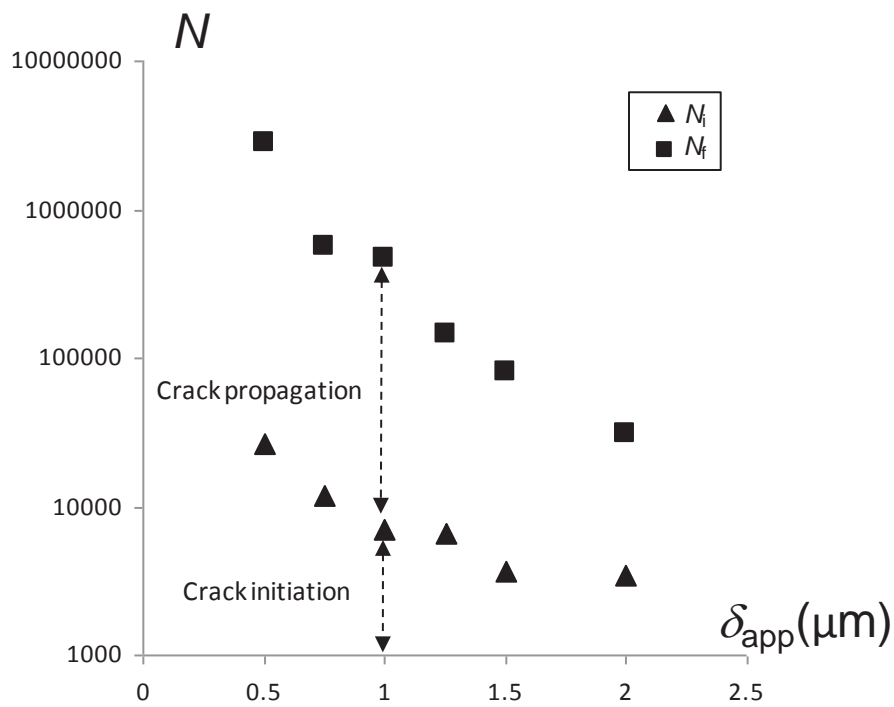
9

10



1
2

(a)



3
4

(b)

5 Figure 21. Comparison of CP-predicted fretting-induced initiation (N_i) and total (N_f) lives as functions of applied tangential displacement for low and high normal loads of (a) $0.5P_y$ and (b) $2P_y$.
6